

## THE DEEP2 GALAXY REDSHIFT SURVEY: COLOR AND LUMINOSITY DEPENDENCE OF GALAXY CLUSTERING AT $Z \sim 1$

ALISON L. COIL<sup>1,2</sup>, JEFFREY A. NEWMAN<sup>3</sup>, DARREN CROTON<sup>4</sup>, MICHAEL C. COOPER<sup>4</sup>, MARC DAVIS<sup>4</sup>, S. M. FABER<sup>5</sup>, BRIAN F. GERKE<sup>4</sup>, DAVID C. KOO<sup>5</sup>, NIKHIL PADMANABHAN<sup>1,3</sup>, RISA H. WECHSLER<sup>6</sup>, BENJAMIN J. WEINER<sup>2</sup>

*Draft version August 20, 2021*

### ABSTRACT

We present measurements of the color and luminosity dependence of galaxy clustering at  $z \sim 1$  in the DEEP2 Galaxy Redshift Survey. Using volume-limited subsamples in bins of both color and luminosity, we find that: 1) The clustering dependence is much stronger with color than with luminosity and is as strong with color at  $z \sim 1$  as is found locally. We find no dependence of the clustering amplitude on color for galaxies on the red sequence, but a significant dependence on color for galaxies within the blue cloud. 2) For galaxies in the range  $L/L^* \sim 0.7 - 2$ , a stronger large-scale luminosity dependence is seen for all galaxies than for red and blue galaxies separately. The small-scale clustering amplitude depends significantly on luminosity for blue galaxies, with brighter samples having a stronger rise on scales  $r_p < 0.5 h^{-1}$  Mpc. 3) Redder galaxies exhibit stronger small-scale redshift-space distortions (“fingers of god”), and both red and blue populations show large-scale distortions in  $\xi(r_p, \pi)$  due to coherent infall. 4) While the clustering length,  $r_0$ , increases smoothly with galaxy color (in narrow bins), its power-law exponent,  $\gamma$ , exhibits a sharp jump from the blue cloud to the red sequence. The intermediate color ‘green’ galaxy population likely includes transitional galaxies moving from the blue cloud to the red sequence; on large scales green galaxies are as clustered as red galaxies but show infall kinematics and a small-scale correlation slope akin to the blue galaxy population. 5) We compare our results to a semi-analytic galaxy formation model applied to the Millenium Run simulation. Differences between the data and the model suggest that in the model star formation is shut down too efficiently in satellite galaxies.

*Subject headings:* galaxies: high-redshift — galaxies: evolution — cosmology: large-scale structure of the universe

### 1. INTRODUCTION

The clustering of galaxies reflects both the spatial distribution of dark matter, which is dependent upon cosmological parameters, and the complex physics which governs the creation and evolution of galaxies within their host dark matter halos. Clustering measures can therefore constrain both cosmology (e.g., Peacock et al. 2001; Abazajian et al. 2005; Eisenstein et al. 2005) and galaxy formation models, including parameterized models like the halo occupation distribution (HOD) models (e.g., Berlind & Weinberg 2002; Yan, Madgwick, & White 2003; Yang et al. 2005; Zehavi et al. 2005; Phleps et al. 2006) or more physical semi-analytic models and hydrodynamic simulations (e.g., Cen & Ostriker 2000; Pearce et al. 2001; Weinberg et al. 2004). In particular, the detailed dependence of clustering on galaxy properties such as luminosity and color at different redshifts provides a wealth of information on galaxy evolution. The formation and evolution of dark matter halos is straightforward to pre-

dict and has been characterized with large N-body simulations (e.g., Mo & White 1996; Sheth, Mo, & Tormen 2001), but the details of how baryons in galaxies populate their parent dark matter halos are less well understood and should depend on the detailed physics of gas accretion, star formation, and feedback processes. Comparisons of the observed dependence of clustering on galaxy properties at different epochs with theoretical models and simulations can illuminate the relative importance of various physical processes involved in galaxy evolution.

On scales of  $\sim 1 - 20 h^{-1}$  Mpc the galaxy two-point correlation function is roughly a power law,  $\xi(r) = (r/r_0)^{-\gamma}$ , and has long been known to depend on galaxy properties, with one of the strongest dependencies being galaxy type. The division of the overall galaxy population into two distinct types has been seen clearly as a function of galaxy morphology, color, and spectral type, where galaxies tend to be either early/bulge-dominated/red/non-star forming or late/disk-dominated/blue/star forming (e.g., Strateva et al. 2001; Madgwick et al. 2002; Blanton et al. 2003a; Kauffmann et al. 2003). Restframe color has been found to correlate well with both spectral type and morphology, with some scatter. In this paper we focus on the dependence of clustering on restframe color, as this quantity can be determined more robustly for large samples of galaxies at both low and high redshift than, for example, morphological type.

The correlation between galaxy type and clustering amplitude was first seen by Davis & Geller (1976) as a difference in the clustering slope of morphologically-

<sup>1</sup> Hubble Fellow

<sup>2</sup> Steward Observatory, University of Arizona, Tucson, AZ 85721

<sup>3</sup> Institute for Nuclear and Particle Astrophysics, Lawrence Berkeley National Laboratory, Berkeley, CA 94720

<sup>4</sup> Department of Astronomy, University of California, Berkeley, CA 94720 - 3411

<sup>5</sup> University of California Observatories/Lick Observatory, Department of Astronomy and Astrophysics, University of California, Santa Cruz, CA 95064

<sup>6</sup> Kavli Institute for Particle Astrophysics & Cosmology, Physics Department, and Stanford Linear Accelerator Center, Stanford University, Stanford, CA 94305

selected elliptical and spiral galaxies, with ellipticals having a steeper slope. This implied that ellipticals are more tightly clustered than spirals and that a neighboring galaxy of an elliptical was more likely to be another elliptical. This was confirmed by Dressler (1980) who found a tight relation between morphology and local galaxy density in clusters of galaxies, with ellipticals preferentially located near the centers of clusters.

The color dependence of galaxy clustering has been measured more precisely in subsequent surveys of the local universe (e.g., Loveday et al. 1995; Hermit et al. 1996; Willmer, da Costa, & Pellegrini 1998), with the most statistically-significant results provided by the latest large surveys, the 2dF Galaxy Redshift Survey (2dFGRS) and the Sloan Digital Sky Survey (SDSS) (Norberg et al. 2002b; Zehavi et al. 2002; Madgwick et al. 2003a; Li et al. 2006a; Zehavi et al. 2005). Table 1 provides an overview of clustering results for color- and spectral type- selected samples from 2dFGRS and SDSS as well as recent intermediate redshift surveys.

In the 2dFGRS, galaxies are classified into early- and late-type using a spectral analysis instead of using rest-frame colors (Madgwick et al. 2002). Madgwick et al. (2003a) find that early-type galaxies are much more strongly clustered than late-type, with a relative bias within spheres of  $8 h^{-1}$  Mpc radius of  $b_{rel} = 1.45 \pm 0.14$ . Norberg et al. (2002b) investigate the luminosity dependence of clustering of early- and late-type galaxies in the 2dF data and find that while there is a strong difference in the relative mix of early- and late-types as a function of luminosity, at  $L > L^*$  this mix is not driving the overall increase of clustering for bright galaxies. Both galaxy types display a clustering increase at higher luminosities, with a constant relative bias between early- and late-types as a function of magnitude at  $L > L^*$ .

These trends are confirmed by Budavari et al. (2003) and Zehavi et al. (2004) using SDSS data. These authors find that both red and blue populations show a significant increase in the correlation length with luminosity, though within the blue cloud there is no significant change in the slope of  $\xi(r)$  for the brighter galaxies. Zehavi et al. (2004) find that within the red population, however, the faintest galaxies ( $-19 < M_r < -18$ ) have a steeper slope, which is likely due to a higher fraction of these galaxies being satellites of central galaxies in groups and clusters (Berlind et al. 2005).

Color dependence of galaxy clustering has been detected in a variety of intermediate redshift ( $0.2 < z < 1$ ) surveys (e.g., Carlberg et al. 1997, 2001; Shepherd et al. 2001; Firth et al. 2002; Phleps et al. 2006). The most robust results to date at  $z \sim 1$  are from the VIMOS-VLT Deep Survey (VVDS; Le Fèvre et al. 2005) and the DEEP2 Galaxy Redshift Survey (Davis et al. 2003). Using VVDS data, drawing from a total sample of 6500 galaxies at  $0 < z < 1.5$  over  $\sim 0.5 \text{ deg}^2$ , Meneux et al. (2006) measure the clustering of red and blue galaxies, dividing the two classes using the observed color bimodality. They find that red galaxies have a higher correlation length and steeper slope than blue galaxies at  $z = 0.8$ , and that the relative bias of red to blue galaxies does not depend significantly on luminosity (Marinoni et al. 2005). These results are consistent with those of Coil et al. (2004b), who use an early DEEP2

data sample of 2200 galaxies at  $0.7 < z < 1.35$  in  $\sim 0.35 \text{ deg}^2$  to determine that galaxies redward of the median color of the sample,  $(B - R)_0 = 0.7$ , have a significantly higher correlation length and steeper slope than bluer galaxies.

Unfortunately, previous studies at intermediate redshift covered relatively small volumes and are dominated by large cosmic variance errors. Here we improve upon earlier  $z \sim 1$  DEEP2 results using the completed DEEP2 data set and volume-limited samples. We measure galaxy clustering in several restframe color bins, with a particular emphasis on ‘green valley’ galaxies at the intersection between the red/early- and blue/late-type populations, and as a function of luminosity within the red and blue galaxy populations separately.

The correlation between galaxy type and clustering strength is also reflected in measurements of the ‘environment’ or local galaxy overdensity around objects of a given class. Locally, Hogg et al. (2003) find a strong relation between local overdensity and galaxy color in SDSS data, on scales of both  $1 h^{-1}$  Mpc and  $8 h^{-1}$  Mpc, with red galaxies favoring more overdense regions. They find little dependence of overdensity on luminosity for galaxies in the blue cloud (though the brightest blue galaxies do appear to be in more overdense regions) and a strong dependence on luminosity for red galaxies locally, with both the brightest and faintest red galaxies being in denser environments than intermediate luminosity red galaxies. The lack of a stronger luminosity-overdensity relation for blue cloud galaxies may be somewhat at odds with the clustering results from 2dF and SDSS, which find a steeper, roughly linear trend of relative bias with magnitude, in that brighter blue galaxies are significantly more clustered than fainter blue galaxies (Norberg et al. 2002b; Zehavi et al. 2005). Swanson et al. (2007), however, also study the clustering of blue galaxies in SDSS and do not find a significant dependence on the relative bias with luminosity, in the same magnitude range as these other local studies, in contrast to the results of Norberg et al. (2002b); Zehavi et al. (2005).

Galaxy overdensity as a function of color and luminosity was recently measured for DEEP2 galaxies by Cooper et al. (2006), who find a similar dependence on color as is seen locally, and a dependence on luminosity for the brightest of the blue galaxies, which lie in overdense regions. No dependence on luminosity was found for galaxies on the red sequence, in the luminosity range probed by DEEP2. We expand upon that study here by measuring the clustering as a function of scale (instead of using a scale-averaged overdensity) using a statistic that may more readily be compared with simulations, as it does not depend upon the bias of the tracer sample used, as is the case with overdensities. The two-point correlation function results presented here will be used for HOD modeling of the galaxy population at  $z \sim 1$  as a function of galaxy type in a future paper.

Significant deviations in the two-point correlation function from a power-law form have recently been detected on scales  $r < 10 h^{-1}$  Mpc for both local and high redshift populations (e.g., Zehavi et al. 2004; Lee et al. 2006; Ouchi et al. 2005; Coil et al. 2006a). These departures from a power law are naturally explained in the HOD framework, which provides a statistical understanding of the relation between galaxies and their dark

matter halos, as the transition between pairs of galaxies within the same halo (the ‘one-halo’ term) on small scales and galaxies in different halos (the ‘two-halo’ term) on larger scales (Zehavi et al. 2004). Small-scale deviations from a power law are expected to be more significant at  $z \geq 1$ , where the exponential tail of the mass function moves to smaller masses, so that at a given mass scale the slope of the mass function becomes steeper (Kravtsov et al. 2004; Conroy, Wechsler, & Kravtsov 2006; Zheng, Coil, & Zehavi 2007). Observationally, deviations are also seen at a given redshift for the brightest galaxy samples, with  $L > L^*$ . This is likely due to the satellite fraction decreasing for brighter samples; brighter galaxies are more likely to be central galaxies than satellite galaxies (Zehavi et al. 2005; Mandelbaum et al. 2006; van den Bosch et al. 2007; Zheng, Coil, & Zehavi 2007), which leads to a steeper one-halo term (Tinker et al, in prep.) as more pairs are central-satellite pairs rather than satellite-satellite pairs and have, on average, a smaller separation.

Departures of the two-point correlation function for DEEP2 galaxies from a power law as a function of luminosity are presented in Coil et al. (2006a); here we perform a similar analysis for galaxies in DEEP2 as a function of color. Given that the galaxy correlation function is not a perfect power law, quoted  $r_0$  and  $\gamma$  fits clearly do not fully capture all of the information present in clustering measures. However, they are still useful as an approximate measure of the amplitude and shape of the correlation function on scales of  $\sim 1 - 10 h^{-1}$  Mpc and facilitate simple comparisons between observational results and models. As such, we provide  $r_0$  and  $\gamma$  fits here but also discuss deviations from a power-law form for the data samples investigated.

The outline of the paper is as follows: §2 briefly describes the DEEP2 survey and defines the data samples used here. In §3 we discuss the methods used in this paper to measure the two-point correlation function, infer the real-space correlation length and slope, and correct for observational biases. §4 presents our results on the color dependence of galaxy clustering at  $z \sim 1$ . In §5 we compare our results with the semi-analytic models of Croton et al. (2006) applied to the Millenium Run dark matter simulation, and we conclude in §6.

## 2. DEEP2 GALAXY SAMPLES

### 2.1. The DEEP2 Galaxy Redshift Survey

The DEEP2 Galaxy Redshift Survey is a recently-completed project using the DEIMOS spectrograph (Faber et al. 2003) on the 10m Keck II telescope to survey optically-selected galaxies at  $z \simeq 1$  in a comoving volume of approximately  $5 \times 10^6 h^{-3} \text{ Mpc}^3$ . Using  $\sim 1$  hour exposure times, the survey has measured high-confidence ( $> 95\%$ , quality flag  $Q = 3$  or 4) redshifts for  $\sim 30,000$  galaxies in the redshift range  $0.7 < z < 1.5$  to a limiting magnitude of  $R_{\text{AB}} = 24.1$ .

The survey covers three deg<sup>2</sup> of the sky over four widely separated fields to limit the impact of cosmic variance. Each field is composed of 2-4 ‘pointings’, each of which covers an area of  $\sim 0.5$  by  $\sim 0.7$  deg, corresponding to the area covered by the CFHT12k camera; there are 10 pointings in total. The DEEP2 spectra have high resolution ( $R \sim 5,000$ ), and rms redshift errors (determined from repeated observations) are  $< 35 \text{ km s}^{-1}$ .

Details of the DEEP2 observations, catalog construction and data reduction can be found in Davis et al. (2003), Coil et al. (2004a), Davis, Gerke, & Newman (2005) and Davis et al. (2007). K-corrections, absolute  $M_B$  magnitudes and restframe ( $U - B$ ) colors have been derived as described in Willmer et al. (2006). We do not include luminosity evolution in the K-corrections for  $M_B$ . Absolute magnitudes given in this paper are in the AB system and are  $M_B - 5 \log(h)$  with  $h = 1$ , which for the remainder of the paper we simply denote as  $M_B$ .

To convert measured redshifts to comoving distances along the line of sight, we assume a flat  $\Lambda$ CDM cosmology with  $\Omega_m = 0.3$  and  $\Omega_\Lambda = 0.7$ . We define  $h \equiv H_0/(100 \text{ km s}^{-1} \text{ Mpc}^{-1})$  and quote correlation lengths,  $r_0$ , in comoving  $h^{-1}$  Mpc.

### 2.2. Galaxy Sample Definitions

From the full flux-limited DEEP2 data set we define a variety of volume-limited subsamples, each corresponding to some range in galaxy ( $U - B$ ) color and  $M_B$  magnitude. A volume-limited sample is not subject to redshift-dependent selection effects, i.e., a galaxy of given rest-frame properties will be within such a sample regardless of its redshift. While volume-limited samples from a given survey will include fewer galaxies than flux-limited samples, they are much easier to interpret and compare with theoretical models, and are therefore used here.

Details of each sample are given in Table 2, and cuts in color, magnitude and redshift are shown in Figure 1. Following Willmer et al. (2006), we define red and blue galaxies using the observed color bimodality in DEEP2 with the following tilted cut in color-magnitude space (in AB magnitudes):

$$(U - B) = -0.032(M_B + 21.62) + 1.035. \quad (1)$$

We do not allow this color cut to evolve with redshift within the redshift range used here. The color samples are shown in Figure 1, where the upper panels are color-magnitude diagrams for all DEEP2 galaxies with  $0.9 < z < 1.0$ . The *main* red and blue samples are defined as those galaxies lying redward or blueward of the line defined in Eqn. 1, with  $M_B < -20$  (dashed lines in the upper left panel of Figure 1) and in the redshift range  $0.7 < z < 0.925$  for red galaxies and  $0.7 < z < 1.05$  for blue galaxies. While the redshift ranges are not identical for the main red and blue samples, differences in their clustering properties are due to the color differences and not the redshift ranges, as we have checked that using the same redshift range for both does not change the results. Using similar redshift ranges also minimizes the effects of cosmic variance, as any density fluctuations will (to first order) be in common between the red and blue samples. We define green galaxies as those within  $(U - B) = 0.1$  of the red/blue dividing line (shown as dot-dash lines in Figure 1) in the redshift range  $0.7 < z < 1.0$ . The green galaxy sample contains a subset of galaxies from each of the red and blue galaxy samples; it is not defined as a distinct set of objects, which would require removing green galaxies from the main red and blue samples.

We further divide the red and blue samples into finer color bins: red galaxies are divided into redder and bluer halves at  $(U - B) = 1.21$ , while blue galaxies are divided into three color samples at  $(U - B) = 0.65$  and

$(U - B) = 0.79$ . These color cuts are shown in the upper right panel of Figure 1. These finer color cuts are independent of magnitude and do not have the a tilt in the color-magnitude diagram, unlike the red/blue dividing line. Our results do not change significantly if we instead define all cuts to be dependent on both color and magnitude. The magnitude range we sample here is not wide, and the number of galaxies near these dividing lines is small enough that it does not significantly affect our results.

Within the red and blue galaxy populations we also construct subsamples as a function of threshold luminosity. For the brighter luminosity samples we allow the upper redshift limit to increase with increasing luminosity, so as to include more galaxies and reduce measurement errors. The lower panels of Figure 1 show  $M_B$  as a function of redshift for red (left) and blue (right) galaxies. The dashed lines indicate the various luminosity samples defined in Table 2. However, as illustrated in Figure 2 of Gerke et al. (2007), the  $R_{AB} = 24.1$  DEEP2 target selection limit defines a restframe color-dependent selection which changes as a function of redshift and which is not evident in Figure 1. Figure 2 of Gerke et al. (2007) contains  $(U - B)$ - $M_B$  color-magnitude diagrams of DEEP2 galaxies in narrow redshift bins of  $\delta z = 0.05$ . The redshift-dependent selection is clearly evident, with the result being that red galaxies are not included in the survey at a given  $M_B$  which is complete for blue galaxies. This results in a lower upper redshift limit of the red samples used here compared to the blue samples of the same luminosity, though the mean redshift of the samples does not vary by more than  $\delta z = 0.2$ .

Number densities for each sample are given in Table 2; these are derived from the DEEP2 luminosity function split by color (Willmer et al. 2006). To account for redshift failures we use ‘minimal’ weighting for the blue galaxies and ‘average’ weighting for the red galaxies (see Willmer et al. (2006) for details). We estimate the number density for the green galaxy sample by multiplying the number densities for the main red and blue samples by the percentage of galaxies in each color that are in the green valley in the redshift range  $0.75 < z < 0.90$  (12.2% of blue galaxies and 21.6% of red galaxies). The dominant error in the number density estimate derived from the luminosity function is the error on  $\phi^*$ ; using the errors quoted in Willmer et al. (2006), the fractional errors on the number densities for the main red and blue samples (with  $M_B < -20.0$ ) are +23%/−5% for blue galaxies and +40%/−55% for red galaxies.

### 2.3. Coadded Spectra

Both locally and to at least  $z = 1$  galaxies are found to be bimodal not only in terms of their restframe color distribution (e.g., Strateva et al. 2001; Blanton et al. 2003a; Bell et al. 2004) but also in morphological and spectral type (e.g., Madgwick et al. 2002, 2003b). Locally, there are strong correlations between morphology, spectral type and restframe color, with some scatter that likely reflects both intrinsic variation and the difficulty of unequivocally determining morphological type. Defining galaxy samples by spectral type in DEEP2 is not as straightforward as using restframe colors (Madgwick et al. 2003b), due to the limited spectral range of the DEEP2 spectra, which is a consequence of

working at high resolution. We therefore define galaxy samples here by restframe color and luminosity; however, we show in Figure 2 coadded rest-frame spectra for galaxies in each of our color samples in order to investigate and illustrate the physical nature of the optical emission for galaxies in each sample. These coadded spectra demonstrate that our color divisions correspond directly to classical spectral types. The coadditions correct for the relative probability that each galaxy was selected for observation by DEEP2, but otherwise all objects are given equal weight. To maximize signal-to-noise and robustness, pixels affected by night sky emission are deweighted and those affected by instrumental artifacts are removed.

The top row of Figure 2 includes the coadded spectra for the main blue and red galaxy samples. The blue galaxies display strong emission lines, primarily from star formation ([OII]  $\lambda 3727$ ,  $H\gamma$ ,  $H\beta$ , [OIII]  $\lambda\lambda 4959, 5007$ ), along with weak Ca H+K  $\lambda\lambda 3934, 3968$  absorption and stronger Balmer absorption features. The main red galaxy sample has a small amount of [OII] and [OIII] emission, primarily from AGN (Yan et al. 2006), as well as Ca H+K absorption and weak Balmer absorption features.

We also show coadded spectra for galaxy samples selected in finer color bins. Within the blue cloud, the bluer galaxies have much stronger star-forming emission lines in equivalent width, while the redder galaxies have lower EW lines; relative to the normalized continuum; in luminosity the redder of the blue galaxies have stronger [OII].

The green galaxies, composed of both blue and red galaxies, have lower EW star-forming lines than the blue galaxies. The green galaxy spectrum does not appear to be a simple mix of the red and blue galaxy spectra, as the line ratios are different. The green galaxy spectrum has a much higher [OIII]/ $H\beta$  ratio than the blue galaxy spectrum or the average of the ‘blue:redder’ and ‘red:bluer’ spectra; this indicates a higher fraction of AGN in the green population relative than in the blue cloud as a whole (Salim et al. 2007; Nandra et al. 2007), and also shows that the green galaxies are not a simple average of the redder of the blue cloud galaxies and the bluer of the red sequence galaxies. The high [OIII]/ $H\beta$  ratio in the green valley population is likely dominated by the red galaxies in the sample (Weiner et al. 2007). Within the red sequence, the bluer galaxies have a higher [OIII]/ $H\beta$  ratio, indicating more AGN activity, and the redder galaxies have stronger Ca H+K absorption features.

## 3. METHODS

### 3.1. Measuring the Two-Point Correlation Function

The two-point correlation function  $\xi(r)$  is defined as a measure of the excess probability  $dP$  (above that for an unclustered distribution) of finding a galaxy in a volume element  $dV$  at a separation  $r$  from another randomly-chosen galaxy,

$$dP = n[1 + \xi(r)]dV, \quad (2)$$

where  $n$  is the mean number density of the galaxy sample in question (Peebles 1980).

For each galaxy sample we construct a randomly-distributed catalog with the same overall sky cover-

age and redshift distribution as the data. We then measure the two-point correlation function using the Landy & Szalay (1993) estimator,

$$\xi = \frac{1}{RR} \left[ DD \left( \frac{n_R}{n_D} \right)^2 - 2DR \left( \frac{n_R}{n_D} \right) + RR \right], \quad (3)$$

where  $DD$ ,  $DR$ , and  $RR$  are counts of pairs of galaxies (as a function of separation) in the data–data, data–random, and random–random catalogs, and  $n_D$  and  $n_R$  are the mean number densities of galaxies in the data and random catalogs. This estimator has been shown to perform as well as the Hamilton estimator (Hamilton 1993) but is preferred here as it is relatively insensitive to the size of the random catalog and handles edge corrections well (Kerscher, Szapudi, & Szalay 2000).

To estimate the cross-correlation function between two galaxy samples, we measure the observed number of galaxies from a given sample around each galaxy in another sample as a function of distance, divided by the expected number of galaxies for a random distribution. For this we use the simple estimator

$$\xi = \frac{D_1 D_2}{D_1 R_2} - 1, \quad (4)$$

where  $D_1 D_2$  are pairs of galaxies between the two samples and  $D_1 R_2$  are galaxy-random pairs between one galaxy sample and the random catalog of the other sample, where the pair counts have been normalized by  $n_D$  and  $n_R$ .

The DEEP2 redshift success rate is >70% overall (defined as the percentage of galaxies targeted for spectroscopy that have a well-determined redshift) and is not entirely uniform across the survey; some slitmasks are observed under better conditions than others and therefore yield a slightly higher completeness. We only use regions of the survey with a redshift success rate >65%, and the spatially-varying success rate is taken into account in the window function, which is applied to the random catalog to ensure that it has the same spatial distribution as the survey. The two-dimensional window function of the DEEP2 data in the plane of the sky reflects the probability of observing a galaxy and takes into account the overall outline of the survey and the geometry of the overlapping slitmasks as well as vignetting in the DEIMOS camera and gaps between the DEIMOS CCDs. The varying redshift success is also taken into account such that regions of the sky with a higher completeness have a correspondingly higher number of random points. This ensures that there is no bias introduced when computing correlation statistics. We also mask the regions of both the random and mock catalogs where the photometric data have saturated stars or CCD defects.

Redshift-space distortions due to peculiar velocities along the line of sight significantly affect estimates of  $\xi(r)$ . At small separations, random motions within a virialized overdensity cause an elongation along the line of sight (“fingers of god”), while on large scales, coherent infall of galaxies into potential wells causes an apparent contraction of structure along the line-of-sight (Kaiser 1987). While these distortions can be used to uncover information about the underlying matter density and thermal motions of the galaxies, they complicate a measurement of the two-point correlation function in real space.

In order to separate the effects of these redshift-space distortions and uncover the underlying real-space clustering properties, we measure  $\xi$  in two dimensions, both perpendicular to and along the line of sight. Following Fisher et al. (1994), we define vectors  $\mathbf{v}_1$  and  $\mathbf{v}_2$  to be the redshift-space positions of a pair of galaxies,  $\mathbf{s}$  to be the redshift-space separation ( $\mathbf{v}_1 - \mathbf{v}_2$ ), and  $\mathbf{l} = \frac{1}{2}(\mathbf{v}_1 + \mathbf{v}_2)$  to be the mean coordinate of the pair. We then define the separation between the two galaxies along ( $\pi$ ) and across ( $r_p$ ) the line of sight as

$$\pi = \frac{\mathbf{s} \cdot \mathbf{l}}{|\mathbf{l}|}, \quad (5)$$

$$r_p = \sqrt{\mathbf{s} \cdot \mathbf{s} - \pi^2}. \quad (6)$$

To estimate  $\xi(r_p, \pi)$ , we apply the Landy & Szalay (1993) estimator to pair counts subdivided over a grid in  $r_p$  and  $\pi$ .

### 3.2. Deriving the Real-Space Correlations

While  $\xi(r_p, \pi)$  contains useful information about peculiar velocities, we also wish to measure the real-space correlation function,  $\xi(r)$ . To recover  $\xi(r)$  we use a projection of  $\xi(r_p, \pi)$  along the  $r_p$  axis. As redshift-space distortions affect only the line of sight component of  $\xi(r_p, \pi)$ , integrating over the  $\pi$  direction leads to a statistic  $w_p(r_p)$ , which is independent of redshift-space distortions. Following Davis & Peebles (1983),

$$w_p(r_p) = 2 \int_0^\infty d\pi \xi(r_p, \pi) = 2 \int_0^\infty dy \xi[(r_p^2 + y^2)^{1/2}], \quad (7)$$

where  $y$  is the real-space separation along the line of sight. If  $\xi(r)$  is modelled as a power law,  $\xi(r) = (r/r_0)^{-\gamma}$ , then  $r_0$  and  $\gamma$  can be readily extracted from the projected correlation function,  $w_p(r_p)$ , using an analytic solution to Equation 7:

$$w_p(r_p) = r_p \left( \frac{r_0}{r_p} \right)^\gamma \frac{\Gamma(\frac{1}{2})\Gamma(\frac{\gamma-1}{2})}{\Gamma(\frac{\gamma}{2})}, \quad (8)$$

where  $\Gamma$  is the usual gamma function. A power-law fit to  $w_p(r_p)$  will then recover  $r_0$  and  $\gamma$  for the real-space correlation function,  $\xi(r)$ .

In practice,  $\xi(r)$  is not expected to be a power law at very large scales ( $\gg 10 h^{-1}$  Mpc), nor can we measure  $\xi(r_p, \pi)$  accurately to infinite separations as assumed in Equation 7. Here we integrate  $w_p(r_p)$  to  $\pi_{\max} = 20 h^{-1}$  Mpc, as  $\xi(r_p, \pi)$  becomes noisy at larger separations. It is not appropriate to then apply equation 8 directly; for power-law correlation functions, that equation becomes increasingly inaccurate at large  $r_p$  (failing significantly where  $r_p/\pi_{\max} \gtrsim 0.25$ ). Instead, we must compare the observed  $w_p(r_p)$  to the integral of  $\xi(r_p, \pi)$  over separations within  $\pi_{\max}$ , as predicted for a given  $r_0$  and  $\gamma$ .

This prediction is complicated by the presence of redshift-space distortions due to coherent infall of galaxies (Kaiser 1987; see Hamilton (1992) and section 4.1 of Hawkins et al. (2003) for the relevant equations for correlation function analyses). If  $\pi_{\max}$  were infinite, these distortions would have no effect, as they merely change the line-of-sight separations of pairs of galaxies; but that is not the case here. The strength of these distortions depends on  $\beta = \Omega_m^{0.6}/b$ , where  $\Omega_m$  is defined at the mean

redshift of the sample (not  $z = 0$ ) and  $b$  is the linear bias between the clustering of galaxies and dark matter.

We therefore recover  $r_0$  and  $\gamma$  as follows. We first measure  $w_p(r_p)$  in the data by integrating  $\xi(r_p, \pi)$  to  $\pi_{\max} = 20 h^{-1}$  Mpc. We then estimate  $w_p(r_p)$  for dark matter particles at the mean redshift of the data sample, using the publicly-available code of Smith et al. (2003) (not including redshift-space distortions), where we integrate the dark matter  $\xi(r_p, \pi)$  to  $\pi_{\max} = 20 h^{-1}$  Mpc. We then estimate the linear galaxy bias from the ratio of these quantities:  $b^2 = [w_p]_{\text{gal}}/[w_p]_{\text{darkmatter}}$ . We use the average value of this  $b$  over scales  $r_p = 1 - 10 h^{-1}$  Mpc and use  $\Omega_m$  at the mean redshift of the sample (for an LCDM model with  $\Omega_m(0) = 0.3$ ), to provide an estimate of the redshift-space distortion parameter  $\beta$ . Using  $\Omega_m(0) = 0.24$  rather than 0.3 increases our recovered  $r_0$  values by 1% and does not change  $\gamma$ . We can then predict the observed  $w_p(r_p)$  for any point in this grid by integrating  $\xi(r_p, \pi)$  to  $\pi_{\max} = 20 h^{-1}$  Mpc. The best-fit  $r_0$  and  $\gamma$  values are those that minimize the  $\chi^2$  difference between the data and the model prediction.

Although our estimated bias, and hence the  $\beta$  used in this procedure, may not perfectly match the bias corresponding to the best-fit values of  $r_0$  and  $\gamma$ , the measured values prove to be insensitive to that estimate. Increasing the bias by 20% increases  $r_0$  by 1% and decreases  $\gamma$  by 1%. This method for recovering  $r_0$  and  $\gamma$  assumes that  $\xi(r)$  is a power law only to a scale of  $\pi_{\max}$  and results in  $r_0$  and  $\gamma$  values within a few percent of those obtained using Equation 8, for our value of  $\pi_{\max} = 20 h^{-1}$  Mpc. Deviations from Equation 8 are significant only on larger scales, where  $r_p/\pi_{\max} \gtrsim 0.25$ . We also consider an alternative method for recovering correlation functions in the next section.

Errors on  $w_p(r_p)$  are calculated using the standard error across the 10 separate data pointings. We do not use a full covariance matrix in the fits. Errors on  $r_0$  and  $\gamma$  are derived from jackknife resampling of the separate pointings and therefore take into account the covariance among the  $r_p$  bins.

### 3.3. Comparison with an Alternative Clustering Statistic

Given that it becomes necessary to model the effects of the truncation of  $w_p$  and include redshift-space distortions when comparing theory with observations, Padmanabhan, White and Eisenstein (2007, hereafter PWE07) propose an alternative statistic,  $\omega(R_s)$ , which has better convergence properties to the real-space quantities. This statistic is defined as

$$\begin{aligned} \omega(R_s) &\equiv 2\pi \int r_p dr_p G(r_p, R_s) w_p(r_p) \\ &= 2\pi \int r_p dr_p G(r_p, R_s) \int_{-\pi_{\max}}^{\pi_{\max}} d\pi \xi(r_p, \pi) \end{aligned} \quad (9)$$

where again  $r_p$  and  $\pi$  are transverse and line of sight directions, respectively. The filter function,  $G(r_p, R_s)$  is chosen to be non-zero only for  $R_s < 1$  and to have zero integral (when integrated against an  $r^2$  measure). We follow PWE07 and adopt  $G(r_p) = R_s^{-3} G(x = r_p/R_s)$  with

$$G(x) = x^4(1 - x^2)^2 \left(\frac{1}{2} - x^2\right) x \leq 1 \quad (10)$$

$$= 0 \quad x > 1. \quad (11)$$

This statistic has the further advantages of being unbinned and having a well-localized kernel in  $\xi(r)$ , probing the correlation function at a scale  $\sim R_s$ . We note that  $\omega(R_s)$  can be thought of as performing the Abel inversion from  $w_p$  to  $\xi$ , while avoiding differentiating noisy data.

In order to test the robustness of the methods presented above, below in Section 4.1 we compute  $\omega$  for the main red and blue galaxy samples to compare with the results obtained using the methods in Section 3.2. To compute  $\omega$  we use the Landy & Szalay (1993) estimator for the two-dimensional correlation function, and the techniques in PWE07 to rewrite the integrals in Eqs. 9 as weighted pair sums; the line of sight integral is truncated at  $\pi_{\max} = 40 h^{-1}$  Mpc. Uncertainties in  $\omega$  are estimated by jackknife resampling the ten DEEP2 pointings. Since  $\omega$  is unbinned, one can choose arbitrarily finely spaced bins, with the disadvantage that adjacent bins become highly correlated. We have verified explicitly that our fits for  $r_0$  and  $\gamma$  given below are insensitive to the particular choice of binning we adopt.

It is straightforward to relate  $\omega$  to the three-dimensional correlation function,  $\xi$ . For a power-law correlation function,  $\xi(r) = (r/r_0)^{-\gamma}$ , and our choice of  $G(r_p, R_s)$ , this relation becomes

$$\omega = \frac{2\pi^{3/2}\Gamma(\frac{\gamma-1}{2})}{\Gamma(\frac{\gamma}{2})} \frac{4(\gamma-1)}{(\gamma-7)(\gamma-9)(\gamma-11)(\gamma-13)} \left(\frac{r_p}{r_0}\right)^{-\gamma}. \quad (12)$$

### 3.4. Systematic Biases due to Slitmask Design

When observing with multi-object slitmasks, the spectra of targets cannot be allowed to overlap on the CCD array; therefore, objects that lie near each other in the direction on the sky that is perpendicular to the wavelength direction on the CCD cannot be simultaneously observed. This results in undersampling the regions of the sky with the highest density of targets. To reduce the impact of this bias, adjacent DEEP2 slitmasks are positioned approximately a half-mask width apart, giving each galaxy two chances to appear on a mask; we also adaptively tile the slitmask locations to hold constant the number of targets per mask. In spite of these steps, the probability that a target is selected for spectroscopy is diminished by  $\sim 25\%$  if the distance to its second nearest neighbor is less than 10 arcseconds (for technical details of the slitmask design, see Davis et al. (2003); Davis, Gerke, & Newman (2005)). This introduces a roughly predictable systematic bias which leads to underestimating the correlation strength on small scales. The objects that are in conflict are often not at the same redshift, however, such that the effect is not particularly large.

To correct for this effect we use the mock catalogs of Yan, White, & Coil (2004) with galaxy colors added as described in Gerke et al. (2007). We measure the ratio of both  $\xi(r_p, \pi)$  and  $w_p(r_p)$  in the mock catalogs between samples of galaxies from catalogs with and without the slitmask target selection algorithm applied. We then multiply the measured  $\xi(r_p, \pi)$  and  $w_p(r_p)$  in the data by this ratio, which is a smooth function of scale and varies from  $\sim 20\%$  on the smallest scales to 2% on scales greater than  $r_p = 1 h^{-1}$  Mpc. We tested mock catalog samples with identical redshift, luminosity and color ranges as

each data sample used here and found no significant differences in the multiplicative corrections as a function of color or luminosity, such that the same correction derived from the largest sample is our best estimate for all other samples. The effect of this slitmask correction is small; it increases  $r_0$  by 1.5% and  $\gamma$  by 2.5%. We include an additional error due to this correction, which is added in quadrature to the error on  $w_p(r_p)$ . This error is estimated from the variance on the correction in the mock catalogs and is a function of scale, varying from 10% at  $r_p = 0.05 h^{-1}$  Mpc to 2% on scales  $r_p > 1 h^{-1}$  Mpc.

#### 4. GALAXY CLUSTERING RESULTS

##### 4.1. Blue and Red Galaxies

We first compare the main blue and red galaxy samples, both of which have  $M_B < -20$ . The top left panels in Figure 3 show  $\xi(r_p, \pi)$  for these two samples, with contours indicating constant probability, where the dark line is  $\xi = 1$ . There are several clear trends present in these diagrams; red galaxies are seen to be more clustered than blue galaxies (a given  $\xi$  is seen at larger separations) and show much stronger fingers of god, as seen in the elongation along the  $\pi$  direction at small  $r_p$  separations ( $< 1 h^{-1}$  Mpc). Both of these results reflect the fact that a color-density relation is in place at  $z \sim 1$ , with red galaxies residing more in overdense regions such as groups and clusters than blue galaxies. Infall on large scales is plainly seen in these  $\xi(r_p, \pi)$  diagrams for blue galaxies, as indicated by the flattening of the contours along the line of sight. Coherent infall may be present for red galaxies as well, though it is harder to detect due to the larger fingers of god (see Section 4.9 for more details). Redshift-space distortions are significant out to  $\pi = 20 h^{-1}$  Mpc, such that it is important to not use the usual power-law estimator (Equation 8) to infer  $r_0$  and  $\gamma$  from  $w_p(r_p)$ , as this equation assumes that one has integrated  $\xi(r_p, \pi)$  to  $\pi = \infty$ .

The top left panel of Figure 4 shows the projected correlation function,  $w_p(r_p)$ , for the main red and blue samples. Red galaxies exhibit a significantly steeper slope than blue galaxies, and both samples are well approximated by a power law within the error bars. Power-law fits are given in Table 2, fitting the data on scales  $r_p = 0.1 - 20 h^{-1}$  Mpc; the smallest  $r_p$  bin ( $0.05 h^{-1}$  Mpc) is not used in these fits due to the rise on small scales which is seen in some samples (see Section 4.3 for further discussion of deviations on small scales). Including the smallest bin in these fits, or fitting only on scales larger than  $r_p = 1 h^{-1}$  Mpc, does not change the results for the main blue and red galaxy samples.

The correlation length for red galaxies is found to be significantly higher than for blue galaxies:  $r_0 = 5.25 \pm 0.26 h^{-1}$  Mpc compared to  $r_0 = 3.87 \pm 0.12 h^{-1}$  Mpc. These values for  $r_0$  at  $z \sim 1$  are somewhat lower than what is found for local samples (Table 1); however,  $r_0$  has only increased by  $\sim 5$ –15% by  $z \sim 0.1$  for blue galaxies and  $\sim 10$ –20% for red galaxies. Furthermore, there has been very little evolution in the slope of the correlation function for either red or blue galaxies since  $z \sim 1$ . We discuss the implications of this in Section 6.

Our  $r_0$  values for blue and red galaxies are somewhat higher than those reported by Coil et al. (2004b) and Meneux et al. (2006), though generally within the large

errors in those findings. Coil et al. (2004b) use early data from a portion of one DEEP2 field and Meneux et al. (2006) use the VVDS Deep Survey first epoch data; both of these samples are roughly 1/6 of the dataset used here, and neither Coil et al. (2004b) nor Meneux et al. (2006) constructs volume-limited subsamples. For blue galaxies, our  $r_0$  value found here is  $2\sigma$  and  $5\sigma$  higher than Coil et al. (2004b) and Meneux et al. (2006), while for red galaxies our  $r_0$  value is  $1\sigma$  and  $2\sigma$  higher, respectively, where the errors have been added in quadrature. Brown et al. (2003) measure the clustering of red galaxies in the NOAO Deep Wide-Field Survey, using photometric redshifts. They find at  $z = 0.85$  that  $r_0 = 6.7 \pm 0.8$  for red galaxies with  $-21.5 < M_R < -20.5$  (roughly  $L/L_*$ ), which is  $2\sigma$  higher than our result. Heinis et al. (2007) measure the clustering of UV-selected galaxies, again using photometric redshifts, and find that at  $z \sim 0.9$   $r_0 = 4.92 \pm 0.5 h^{-1}$  Mpc and  $\gamma = 1.7 \pm 0.09$ . Their clustering scale-length is  $2\sigma$  higher than what we find here for star-forming galaxies.

We also use the estimator of PWE07, as described in Section 3.3, to measure  $\omega$  for the main blue and red samples; the results are shown in Fig. 5. We have not attempted to correct for slitmask effects in the  $\omega$  estimator; these effects are small, as discussed above. Using Eqn. 12, we fit for  $r_0$  and  $\gamma$  for both galaxy samples. The resulting power-law fits are plotted in Fig. 5 (solid lines), and are compared with the fits obtained from fitting to  $w_p$  (dashed lines). The two fits are clearly consistent with each other, given the measurement errors. For the blue galaxy sample, we obtain  $r_0 = 4.45 \pm 0.54 h^{-1}$  Mpc and  $\gamma = 1.47 \pm 0.11$ , while for the red galaxies, we find  $r_0 = 5.94 \pm 0.57 h^{-1}$  Mpc and  $\gamma = 1.93 \pm 0.08$ . These  $r_0$  and  $\gamma$  values are consistent with the estimates derived above from fitting to  $w_p$ . In fact, because the correlation coefficient between  $r_0$  and  $\gamma$  is large and negative ( $\sim -0.8$ ), difference between the results of the two estimators are much less significant than the projected errors imply. The error bars on  $r_0$  and  $\gamma$  are larger using the  $\omega$  estimator, which is not surprising given that  $\omega$  is an inversion of  $w_p$  to a localized integral of  $\xi(r)$ .

##### 4.2. Red-Blue Cross-Correlation

In addition to measuring the auto-correlation of blue and red galaxies separately, the cross-correlation between the two samples can be used to further understand the spatial relationship between blue and red galaxies. The cross-correlation between two samples measures the clustering of one type of object around the other and provides information on the mixing of the populations. On large, linear scales, in the two-halo regime, blue and red galaxies should be well-mixed and trace the same overall large-scale structure, such that the cross-correlation should equal the geometric mean of the auto-correlations of each sample. On small scales, however, within the one-halo term, deviations from the geometric mean encode information about the differences in the halos the two samples populate. For example, if some halos contain almost exclusively red galaxies and others only blue galaxies, then the cross-correlation function would fall below the geometric mean. The blue-red galaxy cross-correlation function can therefore be used to distinguish between different star formation quenching scenarios, as it traces the distribution of quiescent and actively star-

forming galaxies around each other.

Here we measure the cross-correlation of the main blue and red galaxy samples to investigate in particular the mixing of blue and red galaxies on small, one-halo-dominated, scales ( $r_p < 1 h^{-1}$  Mpc). The two-dimensional  $\xi(r_p, \pi)$  cross-correlation function is shown in the lower left panel of Figure 3 and the projected correlation function,  $w_p(r_p)$ , is shown in the upper right panel of Figure 4. The cross-correlation is intermediate between the auto-correlation of blue and red galaxies. The best fit scale length is  $r_0 = 4.37 \pm 0.41 h^{-1}$  Mpc and slope is  $\gamma = 1.83 \pm 0.04$ . Fingers of god are clearly seen in  $\xi(r_p, \pi)$ , though the coherent infall on large scales appears to be more similar to what is seen for the red sample than the blue sample.

Figure 6 shows  $w_p(r_p)$  for the main blue and red galaxy samples and the red-blue cross-correlation function divided by a reference power law  $w_p(r_p)$  with  $r_0 = 4.0 h^{-1}$  Mpc and  $\gamma = 1.8$ . Also plotted are deviations from this power law for the geometric mean:

$$w_p(r_p)_{red-blue} = \sqrt{w_p(r_p)_{red} w_p(r_p)_{blue}}. \quad (13)$$

While the cross-correlation (dot-dash line) is consistent with the geometric mean (dotted line) within the error bars, on scales  $r_p < 1 h^{-1}$  Mpc (the one-halo term) the cross-correlation is closer to the blue  $w_p(r_p)$  than the red. This reflects a deficit of blue galaxies near red galaxies, which could be due to the centers of groups being occupied preferentially by red galaxies. This is consistent with the observed cross-correlation between DEEP2 groups and galaxies (Coil et al. 2006b), which is higher for red galaxies than blue galaxies, again indicating that red galaxies tend to be at the centers of groups.

A similar effect has been seen at  $z = 0.1$  in the SDSS red-blue cross-correlation function. Both Zehavi et al. (2005) and Swanson et al. (2007) find that the red-blue cross-correlation amplitude is lower than the geometric mean of the red and blue clustering on small scales. Wang et al. (2007) measure the cross-correlation as a function of luminosity and find a suppression relative to the geometric mean for faint red and faint blue galaxies, but not for brighter samples. Weinmann et al. (2006b) find a similar effect in their SDSS group catalog, which they term ‘galactic conformity’, in which the colors of satellite galaxies are correlated with the colors of their central galaxies; i.e., red satellite galaxies tend to be around red central galaxies, and the same is seen for blue galaxies.

#### 4.3. Luminosity Dependence for Blue and Red Galaxies

The luminosity dependence of clustering in the overall DEEP2 galaxy sample was presented in Coil et al. (2006a); here we expand upon that study by computing the luminosity dependence of clustering within the blue and red galaxy populations separately. The median  $M_B$  of each sample is given in Table 2. For comparison, at  $z = 0.9$ ,  $M^*$  is  $M_B = -20.54(+0.03/-0.01)$  for blue galaxies and  $M_B = -20.35(\pm 0.03)$  for red galaxies (from Willmer et al. 2006, where we use the ‘minimal’ weighting for blue galaxies and ‘average’ weighting for red galaxies). The main blue sample has a median  $M_B$  value near  $M^*$ , while the blue luminosity subsamples range from 0.44 magnitudes fainter than  $M^*$  to 0.74

magnitudes brighter than  $M^*$ . The main red sample is 0.35 magnitudes brighter than  $M^*$  (in the median) for red galaxies, and the red luminosity subsamples range from  $\sim M^*$  to 1 magnitude brighter than  $M^*$ .

Figures 7 and 8 show  $\xi(r_p, \pi)$  for four luminosity threshold samples for blue and red galaxies. Within the blue population, there is almost no difference between the faintest two samples, while the brightest samples may show somewhat stronger fingers of god. All of the blue luminosity samples show coherent infall on large scales. The red  $\xi(r_p, \pi)$  shows almost no difference between any of the bins; the brightest is noisy, however, due to the small sample size. Any correlation between the strength of the small-scale redshift-space distortion and luminosity within the red galaxy population, for the luminosity range that we probe here, is too weak for us to detect. Li et al. (2006b) find that the pairwise velocity dispersion (see Section 4.8), which quantifies the amplitude of the fingers of god, increases with luminosity for blue galaxies in SDSS, while red galaxies do not show any luminosity dependence, qualitatively similar to our results at  $z \sim 1$ .

The projected correlation function,  $w_p(r_p)$ , is shown in Figure 9 for blue subsamples (top row) and red subsamples (bottom row) as a function of luminosity. Again there is little difference in clustering between the fainter blue samples (upper left panel); however  $w_p(r_p)$  displays a significant rise on small scales for the brighter blue samples (upper right panel). The red samples show no corresponding rise on small scales for the brighter samples (lower right panel). Deviations from a power law for the brighter samples are shown in Figure 10; on scales  $r_p \lesssim 0.2 h^{-1}$  Mpc there is a clear rise in the correlation function of blue galaxies. A similar increase on small scales was seen for all DEEP2 galaxies in Coil et al. (2006a). This is likely due to brighter galaxies having, on average, a higher probability of being a central galaxy rather than a satellite galaxy (Zehavi et al. 2005; Mandelbaum et al. 2006; van den Bosch et al. 2007; Zheng, Coil, & Zehavi 2007), which leads to a relative rise in the one-halo term compared to the two-halo term (Tinker et al, in prep.). There may also be a contribution from interaction-driven starbursts (e.g., Barton, Geller, & Kenyon 2000). The lack of a strong rise on small scales in the brighter red samples likely results from red DEEP2 galaxies having a higher satellite fraction than blue galaxies, at a given luminosity. We note that while the brighter blue galaxies are more likely to be central galaxies, they are not necessarily in more massive halos, as shown by the lack of significant dependence of  $r_0$  on luminosity within the blue cloud.

Power-law fits are given in Table 2 where, as above, the scales used to fit a power law are  $r_p = 0.1 - 20 h^{-1}$  Mpc. Fitting on scales  $r_p = 1 - 20 h^{-1}$  Mpc instead does not significantly change the results. The results are shown in the upper panels of Figure 11. There is no significant dependence in the correlation length,  $r_0$ , or slope,  $\gamma$ , on luminosity for either blue or red galaxies, within the error bars.

Cooper et al. (2006) use local galaxy overdensity measures to determine the environment of DEEP2 galaxies and conclude that within the luminosity range sampled by DEEP2 there is no significant dependence on luminos-



ity for red galaxies, although there is for blue galaxies, in that brighter blue galaxies are in more overdense regions. Within the luminosity range probed here, the relative bias of blue galaxies is found by Cooper et al. (2006) to increase by  $\sim 30\%$ , which is steeper than the trend found here using the correlation function. The brighter blue samples do show an increase in the small-scale clustering amplitude relative to the fainter blue samples, however, which is not reflected in the measured  $r_0$  values. Cucciati et al. (2006) also measure local overdensity at  $z \sim 0.5 - 1.5$  in VVDS data and find that the fraction of red galaxies at a given overdensity depends significantly on luminosity. We do not find such a trend here with our larger dataset.

The lower panels of Figure 11 compare the clustering scale-length of red and blue DEEP2 galaxies as a function of  $L/L^*$  with local results from 2dF (Norberg et al. 2002b) for passive and active galaxies, defined using spectral types, and from SDSS (Zehavi et al. 2005), using restframe colors. For this comparison we use  $M_B^* = -20.67$  for all galaxies at  $z = 0.9$  (Willmer et al. 2006) and  $M_{b_j}^* = -19.66$  and  $M_r = -20.44$  for all galaxies at  $z = 0.1$  (Norberg et al. 2002a; Blanton et al. 2003b). At  $z = 0.1$ , Zehavi et al. (2005); Li et al. (2006a); Wang et al. (2007) all detect significant luminosity dependence in the clustering of both blue and red galaxies, while Swanson et al. (2007) detect luminosity dependence for red galaxies only. Norberg et al. (2002b) detect significant luminosity dependence in the clustering of both passive and active galaxies as well.

This luminosity dependence for local blue and red galaxies is significant at  $L > L^*$  but not at  $L \sim L^*$ ; there is also a significant increase in the clustering for faint red galaxies, but that is below the luminosity range that we probe here. The DEEP2 sample does not probe  $L \gtrsim 2L^*$ , such that we can not test the luminosity dependence at large  $L/L^*$ . Within the range that we do probe, it does not appear that either blue or red galaxies have a detectable luminosity dependence in their autocorrelation properties. This is consistent with local results in the same  $L/L^*$  range.

Our result that the clustering amplitude does not strongly depend on luminosity for red galaxies at  $z \sim 1$  is at odds with Brown et al. (2003), who find a significant luminosity dependence in the clustering of red galaxies at  $z = 0.3 - 0.9$ , for samples between  $M_R = -20$  and  $M_R = -22$  (in Vega magnitudes), using photometric redshift data.  $M_R^*$  for the Brown et al. (2003) sample is  $\sim -21.0$  (M. Brown, private communication). Their value of  $r_0$  at  $z \sim 0.6$  for  $L/L^* \sim 1$  red galaxies is  $6.3 \pm 0.5 h^{-1}$  Mpc, which is only somewhat higher than that found here ( $r_0 = 5.25 \pm 0.26$  at  $\bar{z} = 0.82$ ) or at  $z \sim 0.1$  by Zehavi et al. (2005) ( $r_0 = 5.67 \pm 0.37$ ). However, they find a steep trend in  $r_0$  with  $M_R$ , with  $r_0$  ranging from  $4.4 \pm 0.4 h^{-1}$  Mpc to  $11.2 \pm 1.0 h^{-1}$  Mpc for  $L/L^* \sim 0.4 - 2.5$ , which is not found here or locally. No value of  $M_R^*$  would lead to a consistent trend of  $r_0$  with luminosity when compared with our results or local results from Zehavi et al. (2005) or Norberg et al. (2002b). Estimating  $r_0$  from an angular correlation function, as done in Brown et al. (2003), requires very accurate knowledge of the redshift distribution; this may account for the discrepancy with the results from spec-

troscopic surveys.

Coil et al. (2006a) find that within the full DEEP2 galaxy sample the clustering strength depends strongly on luminosity. This can still occur even if there is no luminosity dependence for red or blue samples separately, as the red galaxy fraction is a function of luminosity; the higher prevalence of red galaxies in the brighter samples leads to  $r_0$  increasing as  $M_B$  decreases.

#### 4.4. Green Galaxies

The clear bimodality both locally and at  $z = 1$  in galaxy properties, whether defined by restframe color, morphology or spectral type, raises the question of how these two main types arise and what, if any, evolutionary connection exists between them. The observed buildup of galaxies on the red sequence since  $z = 1$  (e.g., Bell et al. 2004; Faber et al. 2007; Brown et al. 2007) suggests that blue galaxies are moving to the red sequence with time, though the details of this transition are not clear. The general outline, however, is that star formation begins to shut down or be quenched in blue galaxies, after which they passively evolve onto the red sequence. The star formation quenching process(es) involved may be causally related to the environment of the galaxy (e.g., ram pressure or tidal stripping of gas (Gunn & Gott 1972; Byrd & Valtonen 1990)), such that galaxies in higher density regions end their star forming phase more readily, thus creating a color-density relation. Alternatively, the process may be inherent to the galaxy and depend on its age or stellar or halo mass, in which case the process may be correlated with environment but not caused by it (Bundy et al. 2006; Cooper et al. 2007a). To elucidate what is causing this change, we can investigate the clustering properties of galaxies located at the transition region between these populations. Here we study ‘green’ galaxies located near the minimum of the observed color bimodality as defined in §2.2.

The green galaxy  $\xi(r_p, \pi)$ , shown in the upper right panel of Figure 3, exhibits an intermediate clustering amplitude between the blue and red galaxy samples, as well as intermediate-strength fingers of god. The green population displays somewhat similar infall on large scales as blue galaxies, though the contours are noisy on large scales due to the relatively small sample size.

The projected correlation function for green galaxies is shown in the lower left panel of Figure 4, plotted with  $w_p(r_p)$  for red and blue galaxies for comparison. On large scales ( $r_p > 1 h^{-1}$  Mpc) the green galaxies have a clustering amplitude similar to that of red galaxies, while on small scales the amplitude is closer to that of blue galaxies. The large-scale agreement with the red galaxy population implies that green galaxies reside in or on the outskirts of halos of similar mass as red galaxies, as they have the same clustering for the two-halo term. Green galaxies are therefore generally in the same overdense regions as red galaxies. However, the one-halo term for green galaxies is lower than for red galaxies, which likely reflects a lower radial concentration of green galaxies within their parent halos. The overall picture is consistent with galaxies having green colors while on the outskirts of halos and becoming redder as they reach the center of the overdensity. These results point towards green galaxies being a distinct population and not a sim-

ple mix of red and blue galaxies.

To investigate these trends further, we compute the cross-correlation between the green galaxy sample and the main blue and red galaxy samples. The  $\xi(r_p, \pi)$  diagrams (lower right panels of Figure 3) show more significant infall on large scales in the green-blue cross-correlation than the green-red cross-correlation (comparing, for example, the  $\xi = 1$  contours). The green-red cross-correlation is very similar to the blue-red cross-correlation (though with smaller fingers of god), indicating that green galaxies have comparable kinematics to blue galaxies. There are also smaller fingers of god in the green-red cross-correlation than in the red auto-correlation. These results are consistent with green galaxies residing in the same overdense regions as red galaxies, on average, but with a lower probability of being at the cores of those overdensities, compared to red galaxies. This would result in green galaxies having smaller fingers of god than red galaxies, and a lower auto-correlation on small scales. It is possible that green galaxies reside on the outskirts of the same halos that red galaxies occupy but are still falling in towards the centers of the halos.

The bottom right panel of Figure 4 shows the projected cross-correlation functions between green and blue or red galaxies. The green-red galaxy clustering amplitude is higher than the green-blue galaxy amplitude on all scales. On scales  $r_p = 1 - 10 h^{-1}$  Mpc the green-red sample is  $39 \pm 5\%$  more clustered. On small scales, dominated by the one-halo term, the green-red amplitude is a few times higher than the green-blue amplitude: a factor of  $2 \pm 0.2$  times higher on scales  $\sim 0.5 h^{-1}$  Mpc and a factor of  $2.8 \pm 0.4$  times higher on scales  $\sim 0.25 h^{-1}$  Mpc. One would therefore be *much* more likely to find a red close neighbor (or satellite) galaxy to a green galaxy than a blue neighbor, and vice versa, if red and blue galaxy samples were of equal size. Another way to frame these results is that a green galaxy is less likely to be a central galaxy than a red galaxy of similar luminosity, but more likely than a comparable blue galaxy.

We note that the green galaxy  $w_p(r_p)$  likely can not be fit with an HOD model that assumes that the radial distribution of galaxies follows that of dark matter particles or subhalos. The green galaxy radial distribution is clearly different from that of either red or blue galaxies, and most HOD models do not allow the radial distribution to vary for different galaxy types.

#### 4.5. Finer Color Bins

We next divide the blue and red galaxy samples into finer color bins to investigate the strength of clustering as a function of color *within* each population. Figure 12 shows  $r_0$  and  $\gamma$  as a function of color for both the main blue and red samples (triangles), the green sample, and for finer color bins. As explained in Section 2.2, the finer color bins are not all independent; this is shown in the figure with a dotted horizontal line showing the color range for each point (for clarity the color ranges for the main blue and red samples are omitted). In particular, the green galaxy sample contains subsamples of both blue and red galaxies.

Within the red population (where we have two independent samples) neither  $r_0$  or  $\gamma$  depend significantly on color; across the red sequence we detect no change in

the clustering properties of galaxies. Within the blue population, however, there is a strong dependence; redder galaxies are more clustered than the bluer galaxies. There is no corresponding trend seen in the slope of the correlation function. The abrupt change in slope between blue and red galaxies likely reflects the different radial concentrations and satellite fractions of the two populations and may indicate that star formation quenching is an effect associated with the halo properties of galaxies.

Interestingly, the green galaxy  $r_0$  is found to be the same as the red galaxy  $r_0$  (within  $1 \sigma$ ), while the green galaxy  $\gamma$  is the same as for blue galaxies, not red galaxies. This is consistent with the interpretation in the previous section that green galaxies reside in similar mass halos as red galaxies, and are found generally in overdense regions, but are less concentrated within their host halos than red galaxies. They apparently do not populate the centers of overdensities.

As discussed earlier, luminosity function studies find that a significant fraction of the progenitors of local galaxies on the red sequence must have been in the blue cloud at  $z \sim 1$  (Bell et al. 2004; Brown et al. 2007; Faber et al. 2007). Our clustering results imply that the galaxies that migrate to the red sequence from  $z = 1$  to  $z = 0$  are amongst the redder of the blue galaxies, and the green galaxies at  $z = 1$ , which are already as clustered as galaxies on the red sequence.

These trends of finding a color-density relation within the blue cloud but not within the red sequence are similar to what has been locally using galaxy environment measures (e.g., Hogg et al. 2003, 2004). There are no other published  $z \sim 1$  clustering results with such fine color bins to compare to, and we defer a comparison with the DEEP2 environment results of Cooper et al. (2006) to Section 4.7.

#### 4.6. Galaxy Bias and Relative Bias Between Samples

To facilitate comparisons to published clustering results measured at other redshifts or with different statistics than the two-point correlation function, we calculate the relative bias between various galaxy color samples. We define the relative bias as the square root of the ratio of  $w_p(r_p)$  for two samples. As the relative bias is scale-dependent, we calculate the mean relative bias over two scales,  $r_p = 0.1 - 15 h^{-1}$  Mpc ('all scales') and  $r_p = 1 - 15 h^{-1}$  Mpc ('large scales'), which have mean scales of  $r_p = 4.4 h^{-1}$  Mpc and  $r_p = 6.5 h^{-1}$  Mpc, respectively.

The relative bias of red to blue galaxies is  $b_{rel} = 1.28 \pm 0.09$  on large scales and  $b_{rel} = 1.44 \pm 0.07$  on all scales, reflecting the rise in the relative bias on small scales,  $r_p < 1 h^{-1}$  Mpc. We do not find any dependence on luminosity for the relative bias between red and blue galaxies. This is in contrast to the results of Cucciati et al. (2006), who measure the color-density relation at  $z \sim 0.5 - 1.5$  in VVDS data and find that the color-density relation steepens for brighter galaxies. No such trend is detected here.

The lack of luminosity dependence in the relative bias found here could indicate that the ratio of the satellite fraction in red versus blue galaxy samples does not depend on luminosity. Berlind et al. (2005) show that for central galaxies there is no color-density relation; this relation only exists for satellite galaxies. This implies

that the relative bias of red to blue galaxies should be a function of luminosity if the central to satellite galaxy fraction changes with luminosity differentially for red and blue galaxies. The fact that the data show no dependence in the relative bias on luminosity could imply that the ratio of the satellite fraction in red versus blue galaxy samples is fixed and does not depend on luminosity.

The relative bias of red to green galaxies is  $b_{rel} = 1.00 \pm 0.10$  on large scales and  $b_{rel} = 1.12 \pm 0.11$  on all scales. Given that red and green galaxies have different correlation slopes and redshift-space distortions, the relative bias does not fully reflect the differences between these populations. It does, however, indicate that when two-halo-dominated scales are included, on average the clustering amplitude of green galaxies is perfectly consistent with that of red galaxies and is not lower. The relative bias of green to blue galaxies is found to be  $b_{rel} = 1.30 \pm 0.11$  on both large and all scales, with no scale-dependence.

The relative bias found here between red and blue galaxies at  $z \sim 1$  is very similar to what is measured at lower redshift (see Table 1;  $b_{rel}$  is  $\sim 0 - 10\%$  lower at  $z \sim 1$ ). Madgwick et al. (2003a) compare the clustering of early and late type galaxies (defined by spectral type) and find a relative bias of  $b_{rel} = 1.45 \pm 0.14$  integrated to scales of  $r = 8 h^{-1}$  Mpc, while Willmer, da Costa, & Pellegrini (1998) find a relative bias of  $\sim 1.4$  between red and blue galaxies. Zehavi et al. (2002) find using SDSS data that the relative bias of red to blue galaxies is  $\sim 1.6$ , but is highly scale-dependent. This agreement with lower redshifts implies that the dependence of color on density at  $z = 1$  is as steep as it is locally; the physical mechanisms responsible for the color-density relation are just as effective before  $z = 1$  as they are after. The color-density relation was therefore established before  $z = 1$  and subsequent changes may be absolute (in terms of the zeropoint of the relation) but not relative (which would change the slope), within the errors. As discussed in Cooper et al. (2006), given the low abundance of rich clusters at  $z = 1$ , the color-density relation seen in the DEEP2 data can not be the result of cluster-specific physics such as ram pressure stripping of gas or galaxy harassment (e.g., Gunn & Gott 1972; Byrd & Valtonen 1990).

For a given cosmology we can also compute the *absolute* galaxy bias relative to the underlying dark matter density field using results from N-body simulations. We use the power spectrum of Smith et al. (2003) to estimate the dark matter clustering amplitude at the same redshift as the data, for a cosmology with  $\Omega_m = 0.3, \Omega_\Lambda = 0.7, \sigma_8 = 0.9$ , and  $\Gamma = 0.21$ . This code is an analytic fit motivated by the halo model; we include a 5% error on the dark matter  $w_p(r_p)$  at each scale in our calculation of the absolute bias to reflect the uncertainty in the fit. The resulting absolute bias values averaged on scales  $r_p = 1 - 10 h^{-1}$  Mpc are listed for each color and magnitude sample in Table 2. For  $\sigma_8 = 0.8$  the large-scale bias is 13% higher, while for  $\sigma_8 = 1.0$  it is 10% lower. Note that the absolute bias and relative bias are measured on different scales.

We find that the absolute bias is  $b = 1.65 \pm 0.15$  for red galaxies and  $b = 1.28 \pm 0.04$  for blue galaxies, both with  $M_B < -20.0$ . This is consistent with Marinoni et al. (2005), who find that red galaxies with

$M_B < -20.0$  at  $z \sim 0.8$  have an absolute bias of  $b = 1.5 \pm 0.6$  and blue galaxies have  $b = 1.1 \pm 0.6$ , measured on scales of  $r = 8 h^{-1}$  Mpc. The absolute bias of galaxies at  $z \sim 1$  measured here is higher than at  $z = 0$  (e.g., Verde et al. 2002; Hoekstra et al. 2002; Seljak et al. 2005; Simon et al. 2007), where galaxies near  $L^*$  are found to have a bias of  $b \lesssim 1.0$ .

#### 4.7. Comparison to Environment Studies

To compare our results on the color dependence of galaxy clustering with the DEEP2 environment results of Cooper et al. (2006), we show in Figure 13 the relative bias of each color sample used here, relative to the main blue sample, measured on scales  $r_p = 1 - 5 h^{-1}$  Mpc. The main red and blue samples are shown as triangles, while the finer color bins are shown as diamonds. Crosses with dotted error bars are the relative galaxy overdensity as measured by the environment statistic  $\delta_3$  (described in Cooper et al. (2006)) for galaxies with  $z = 0.75 - 1.0$  and  $M_B < -20.0$ , as a function of color, again normalized to the main blue sample. Note that this redshift and magnitude range are not exactly the same as those used in Cooper et al. (2006), therefore our Figure 13 does not look identical to Figure 5 in Cooper et al. (2006).

The overall agreement is very good between the relative overdensity and the relative bias from the clustering measures presented here; these two statistics should be similar but not identical. The overdensity estimate,  $\delta_3$ , is not measured at a fixed scale but is generally in the range  $r = 1 - 3 h^{-1}$  Mpc; we compare to the relative bias from clustering averaged on scales  $r_p = 1 - 5 h^{-1}$  Mpc to minimize systematics from scale dependence. The environment overdensity statistic is in some ways a scale-averaged clustering measure, so the agreement between the two should be good. However, the environment statistic uses *all* neighboring galaxies to define the local overdensity, not just those with the same color or magnitude as the galaxy for which one is measuring the environment. This is different from the clustering statistic we use, where only galaxies within a given color and magnitude range are used for the auto-correlation function. Using all galaxies as a density tracer could potentially cause the environment statistic to be more sensitive to group membership and corresponding small-scale overdensities for populations which tend to be central galaxies instead of satellite galaxies (i.e., if there is only one galaxy of that type in an overdensity).

As seen in Figure 13, the agreement between the two statistics is good but not exact. In particular, the clustering results show a continued trend within the blue population of the bluest galaxies being the least clustered, which is not clearly reflected in the environment measure, though the discrepancy is at the  $1\sigma$  level; the broader environment samples in Cooper et al. (2006) do show such a downturn.

Our clustering-based results on the color-density relation at  $z \sim 1$  are very similar to local environment findings in SDSS. Hogg et al. (2003, 2004) find that SDSS galaxies also show a color-density relation within the blue population, but not within the red sequence. They also find that locally the overdensity of blue galaxies shows little luminosity dependence, while there is strong luminosity dependence within the red galaxy population.

Unfortunately, the DEEP2 volume is not large enough to provide a fair sample of the brightest, rarest red galaxies at  $z \sim 1$ , and the error bars on our results for  $r_0$  as a function of luminosity within the red sequence are 5-15%, which may be large enough to mask a modest luminosity dependence for the range of luminosities we probe. The general conclusion is that there has not been qualitative evolution in the color-luminosity-overdensity space since  $z \sim 1$ .

#### 4.8. Pairwise Velocity Dispersion

On small scales ( $r \lesssim 1 h^{-1}$  Mpc) random motions within galaxy groups and clusters lead to elongations of the  $\xi(r_p, \pi)$  contours along the line of sight, the so-called ‘‘fingers of god’’. These motions can only be seen in spectroscopic redshift surveys, and at  $z \sim 1$  only the DEEP2 and VVDS surveys can currently detect these distortions in  $\xi(r_p, \pi)$ . The virialized motion of the galaxies can be measured using the pairwise velocity dispersion,  $\sigma_{12}$ , which is estimated by modeling  $\xi(r_p, \pi)$  as a convolution of the real-space correlation function,  $\xi(r)$ , with a broadening velocity function. The relation between  $\xi(r_p, \pi)$  and  $\xi(r)$  is usually assumed to be

$$1 + \xi(r_p, \pi) = \int f(v_{12}) \left[ 1 + \xi(\sqrt{r_p^2 + y(v_{12}, \pi)^2}) \right] dv_{12}, \quad (14)$$

where  $f(v_{12})$  is the distribution function of the relative velocity difference between galaxy pairs along the line of sight (e.g., Davis & Peebles 1983). This velocity difference is defined as

$$v_{12} \equiv \pi - y + \bar{v}_{12}(r) \quad (15)$$

where  $\bar{v}_{12}(r)$  is the mean radial pairwise velocity of galaxies at separation  $r$  and  $y$  is the real-space separation along the line of sight. Here  $y$  has units of  $\text{km s}^{-1}$  instead of  $h^{-1}$  Mpc (this conversion includes a factor of  $H_0$ , with  $h = 1$ , and a factor of  $(1+z)$ ), such that the same physical velocity at  $z = 1$  has less of an effect on  $\xi(r_p, \pi)$  than at  $z = 0.1$ .

To measure the small-scale velocity dispersion on scales  $r \sim 1 h^{-1}$  Mpc, we follow Fisher et al. (1994) and in Equation 14 we use

$$\xi(r_p = 1, \pi) \equiv 0.5[\xi(r_p = 0.5 \text{Mpc } h^{-1}, \pi) + \xi(r_p = 1.5 \text{Mpc } h^{-1}, \pi)] \quad (16)$$

in both real and redshift space, for values of  $\pi \leq 20 h^{-1}$  Mpc. We then normalize  $\xi(r_p = 1, \pi)$  so that our subsequent fitting will be sensitive to the overall shape of  $\xi(r_p = 1, \pi)$  but insensitive to the amplitude.

An exponential form is usually adopted for  $f(v_{12})$  (e.g., Davis & Peebles 1983; Fisher et al. 1994; Diaferio & Geller 1996; Sheth 1996):

$$f(v_{12}) = \frac{1}{\sqrt{2}\sigma_{12}} \exp\left(-\frac{\sqrt{2}}{\sigma_{12}} |v_{12} - \bar{v}_{12}|\right), \quad (17)$$

where  $\bar{v}_{12}$  is the mean and  $\sigma_{12}$  is the dispersion of the pairwise peculiar velocities. We assume an infall model based on the similarity solution of the pair conservation equation (Davis & Peebles 1977),

$$\bar{v}_{12}(\mathbf{r}) = -\frac{y}{1 + (r/r_*)^2}, \quad (18)$$

where  $r_* = 5 h^{-1}$  Mpc and  $y$  is the radial separation in the real space. The results are relatively insensitive

to the assumed model;  $\sigma_{12}$  is  $\sim 20\text{-}40\%$  lower if  $\bar{v}_{12}$  is assumed to be negligible.

To estimate  $\sigma_{12}$ ,  $\xi(r)$  is modelled using the power-law fits for  $r_0$  and  $\gamma$  for each sample, and we minimize  $\chi^2$  between the observed  $\xi(r_p = 1, \pi)$  and modelled  $\xi(r_p = 1, \pi)$  for a range of  $\sigma_{12}$  values. The results are given Table 2, where errors are derived from jackknife samples. Red galaxies are found to have  $\sigma_{12} = 530 \pm 50 \text{ km s}^{-1}$ , while blue galaxies have a significantly lower value of  $\sigma_{12} = 240 \pm 20 \text{ km s}^{-1}$ . The error bars are too large to detect significant differences as a function of luminosity within the red or blue galaxy populations or as a function of color for the finer color bins. Green galaxies have a large value,  $\sigma_{12} = 490 \pm 110 \text{ km s}^{-1}$ , consistent with red galaxies and  $2\sigma$  larger than blue galaxies.

These numbers are similar to, but somewhat smaller than, values found at  $z = 0.1$ . Using the same infall model, Zehavi et al. (2002) measure  $\sigma_{12} \sim 650 - 750 \text{ km s}^{-1}$  for red galaxies in SDSS and  $\sigma_{12} \sim 300 - 450 \text{ km s}^{-1}$  for blue galaxies at  $z = 0.1$ . Li et al. (2006b) also find for SDSS galaxies that  $\sigma_{12} \sim 600 - 800 \text{ km s}^{-1}$  for red galaxies and  $\sigma_{12} \sim 200 - 400 \text{ km s}^{-1}$  for blue galaxies. Madgwick et al. (2003a) measure similar values for galaxies in the 2dF Redshift survey:  $\sigma_{12} = 612 \pm 92 \text{ km s}^{-1}$  for passive galaxies (defined by spectral type) and  $\sigma_{12} = 416 \pm 76 \text{ km s}^{-1}$  for active, star-forming galaxies.

Our finding that red galaxies have stronger fingers of god at  $z \sim 1$  than blue galaxies again reflects the result that, on average, red galaxies reside in more overdense regions, such as galaxy groups, than blue galaxies.

#### 4.9. Multipole Moments

Peculiar velocities also affect  $\xi(r_p, \pi)$  on large scales, where coherent infall of galaxies onto forming structures flattens  $\xi(r_p, \pi)$ . A standard method for quantifying these large-scale redshift-space distortions is to measure the ratio of the quadrupole to monopole moments of the two-point correlation function (Hamilton 1992). The two-dimensional correlation function can be decomposed into a sum of Legendre polynomials,

$$\xi(r_p, \pi) = \sum_l \xi_l(s) \mathcal{P}_l(\mu), \quad (19)$$

where  $\mathcal{P}_l$  is the  $l^{\text{th}}$  Legendre polynomial and  $\mu$  is the cosine of the angle between the line of sight and the redshift separation vector,  $\mathbf{s}$ . The multipole moments are defined as

$$\xi_l(s) = \frac{2l+1}{2} \int_{-1}^1 \xi(r_p, \pi) \mathcal{P}_l(\mu) d\mu. \quad (20)$$

Following Hamilton (1992), we define

$$Q(s) \equiv \frac{\xi_2(s)}{(3/s^2) \int_0^s \xi_0(s') s'^2 ds' - \xi_0(s)}. \quad (21)$$

This ratio depends on  $\beta \equiv \Omega_M^{0.6}/b$ , where  $b$  is the linear galaxy bias (Kaiser 1987), as

$$Q(s) = -\frac{(4/3)\beta + (4/7)\beta^2}{1 + (2/3)\beta + (1/5)\beta^2}. \quad (22)$$

Figure 14 shows  $Q(s)$  for the main blue and red galaxy samples.  $Q(s)$  is positive on small scales where the fingers of god are strong and negative on large scales where

coherent infall dominates. The dotted lines indicate  $Q$  predicted on linear scales (from Equation 22), assuming  $\Omega_m$  at the mean redshift of each sample (for the blue sample  $\Omega_m(z = 0.90) = 0.75$  and for the red sample  $\Omega_m(z = 0.82) = 0.72$ , corresponding to  $\Omega_m(z = 0) = 0.3$ ) and using the inferred linear galaxy bias for each sample,  $b = 1.28$  for blue galaxies and  $b = 1.65$  for red galaxies. Using  $\Omega_m(z = 0) = 0.24$  increases the predicted  $Q$  values by  $\sim 5\%$ . For the blue sample  $\beta = 0.66$  and for the red sample  $\beta = 0.50$ . Both galaxy samples have negative  $Q$  values, on scales  $s > 5 h^{-1}$  Mpc for blue galaxies and  $s > 10 h^{-1}$  Mpc for red galaxies, indicating coherent infall, though the significance is lower for red galaxies. On the largest scales  $Q$  increases; however, the error bars increase on these scales as well, which approach the transverse scale of the survey and so may be susceptible to systematic effects. On scales  $s \sim 10 - 15 h^{-1}$  Mpc the blue sample is consistent with the predicted constant  $Q$  value within the noise. The red sample does not reach the predicted negative value on the largest scales; however, given the non-negligible pairwise velocity dispersion we do not expect this model to be perfect, as even on scales of  $15 h^{-1}$  Mpc,  $Q(s)$  is sensitive to  $\sigma_{12}$  and the form of  $f(v_{12})$ . This is especially true for the red galaxy sample, where  $\sigma_{12}$  is greater. The fact that infall is seen indicates that the clustering of galaxies is dynamic and growing, as expected.

## 5. COMPARISON WITH SEMI-ANALYTIC MILLENNIUM RUN SIMULATION

We compare our clustering results for blue and red galaxies with the recent semi-analytic galaxy formation model of Croton et al. (2006) applied to the Millennium Run N-body dark matter simulation (Springel et al. 2005). The Millennium Run follows the dynamical evolution of  $10^{10}$  dark matter particles in a periodic box of side-length  $500 h^{-1}$  Mpc with a mass resolution per particle of  $8.6 \times 10^8 h^{-1} M_\odot$ . Cosmological parameters consistent with those measured from the first year WMAP data (Spergel et al. 2003; Seljak et al. 2005) were used. The galaxy formation model follows the growth of approximately 25 million galaxies from their birth to the present day and has been tuned to provide a good match to many observed properties of local galaxies, primarily the luminosity function and Tully-Fisher relation. Within this model the behavior of the observed global galaxy two-point correlation function is well reproduced at  $z = 0$ , however when split by galaxy color,  $z = 0$  red galaxies are somewhat too clustered in the model while blue galaxies are under-clustered (Springel et al. 2005). Ours is the first test of the clustering of Millennium Run galaxies as a function of color at higher redshift.

Using an ensemble of 15 light-cones, each of which matches the geometry of one of the four DEEP2 survey fields (see Kitzbichler & White 2007, for further details) we measure the clustering of blue and red galaxies with the same  $M_B$  and  $z$  ranges as our main DEEP2 color samples. We define galaxies to be blue or red in the model using the same color cut as used for DEEP2 galaxies (Equation 1). If we instead use the minimum of the observed color bimodality in the model galaxies (which is roughly 0.1 mags blueward of the location for the DEEP2 galaxies) our qualitative results and conclusions remain unchanged. Details of each sample used in

the mock catalogs are given in Table 2. The number densities for red and blue galaxies in the model match the observed number densities quite well.

The resulting  $\xi(r_p, \pi)$  contours for the semi-analytic model galaxies are shown in Figure 15. Red model galaxies are more clustered and have stronger fingers of god than the blue model galaxies. A direct comparison between the red model galaxy  $\xi(r_p, \pi)$  and the equivalent DEEP2 result (Figure 3) indicates that a) the redshift-space distortions are generally similar between the model and data, including both the fingers of god and the coherent infall on large scales, and that b) the overall clustering amplitude is larger in the model; e.g. compare the thick  $\xi = 1$  lines. Hence, the discrepancy seen at  $z = 0$  appears to extend back to earlier epochs. The blue model galaxy  $\xi(r_p, \pi)$  shows differences with the data as well. The left panel of Figure 15 shows coherent infall on large scales but no small-scale redshift-space distortions, unlike the DEEP2 data. This is reflected in the low value of  $\sigma_{12}$  found for the model blue galaxies (see Table 2).

The discrepancies seen in Figure 15 are highly significant, as seen in the projected correlation functions shown in Figure 16, where the observed DEEP2 results are shown for comparison. On scales  $r_p < 0.5 h^{-1}$  Mpc the blue cloud semi-analytic model correlation function is flat and does not continue to rise as in the data. In addition, in the quasi-linear regime,  $r_p = 1 - 10 h^{-1}$  Mpc, the blue model galaxies are less clustered than the data by  $\sim 15\%$ . In contrast, the red galaxies in the model are significantly more clustered than the data,  $\sim 40\%$  over most scales, as also seen at low redshift. Power-law fits are given in Table 2, where slightly larger scales are used for the model fits ( $r_p = 0.4 - 20 h^{-1}$  Mpc) than for the data, as the model blue galaxy  $w_p(r_p)$  is not a power law on smaller scales.

Finally, the red-blue cross-correlation function for the model galaxies is shown in Figure 17 (solid line) along with the cross-correlation function in the DEEP2 data (thin dashed line) and the geometric mean of the red and blue auto-correlation functions in the model (dot-dash line). The cross-correlation function in the model is clearly lower on small scales ( $r_p < 1 h^{-1}$  Mpc) than either the geometric mean or the DEEP2 data. This reflects the lack of blue galaxies around red galaxies in the model. Interestingly, a hint of this same flattening of  $w_p(r_p)$  for blue galaxies in this model can be seen at  $z = 0$  in Figure 5 of Springel et al. (2005); however they do not plot below scales  $r_p = 0.5 h^{-1}$  Mpc where for us the effect is most pronounced.

It appears that the discrepancies shown in Figures 16 and 17 are due to the incorrect modeling of the physics that determines the colors of satellite galaxies. If too few model satellite galaxies are blue compared to the data at  $z \sim 1$ , then both the model blue auto-correlation function and red-blue cross-correlation function will have lower amplitudes on small scales than seen in the DEEP2 data, inside the ‘one-halo’ regime ( $r_p < 1 h^{-1}$  Mpc). Similarly, an overabundance of red satellites on such scales should also be present, as is seen in Figure 16.

A similar effect is detected at low redshift when comparing the fraction of blue SDSS galaxies in groups with these Millennium Run semi-analytic models. Weinmann et al. (2006a) find that the blue fraction of galaxies in groups is much higher in the SDSS data than

in the model, which predicts at  $z = 0.1$  that almost all satellite galaxies ( $\sim 85\%$ ) are red.

Our results provide a valuable way to test some of the physical assumptions made by the semi-analytic model to better understand the processes that may actually be occurring and their relative importance. We identify two overly simplified aspects of the model satellite evolution that contribute to the clustering discrepancies shown in Figure 16. The first is the way in which hot gas is stripped from halos ( $M_{\text{halo}} \gtrsim 10^{12} h^{-1} M_{\odot}$ ) when the halo falls into the potential of a more massive system. As discussed by Weinmann et al. (2006a), the common assumption in most semi-analytic models is one of *extreme strangulation*, where all of the hot gas is instantly stripped and added to that of the larger halo upon accretion. This simplifying assumption is important for galaxy colors because the dynamical time for a sub-halo (and hence satellite galaxy) to merge is usually longer than the time it takes the stellar population to fade and redden, which all model satellites will do in the absence of fresh fuel for star formation. This provides an overly-efficient channel for blue satellites to transform into red satellites.

Weinmann et al. (2006a) point out that the Croton et al. (2006) model does not include a host halo mass dependence for the strangulation efficiency. Given that the ability of a parent halo to strip gas from a subhalo likely depends on the density of the hot gas in the parent halo, a model which includes such a mass-dependent strangulation prescription might provide a better match to the results shown here.

The second aspect of the model satellite evolution that may be discrepant with the real universe is the assumption that local potential wells (i.e. subhalos inside larger parent halos) cannot accrete gas, meaning that after a satellite galaxy is captured by the larger halo it receives no new baryonic fuel for later star formation from the intragroup or intracluster medium. This may be generally true in N-body simulations which show that subhalos tend to lose mass through tidal stripping as they spiral inward, not gain mass. However it is plausible that in the outer regions of a dark matter halo, the local potential of a subhalo may dominate that of its host and attract new baryons from the hot parent halo, baryons that may subsequently cool onto the satellite. Such gas would extend the star formation history of the satellite and hence modify the evolution of its color.

It is also important to note that there are processes that are known to operate in cluster (and also group) environments that act to remove cold gas from a satellite galaxy, such as tidal stripping and harassment. These processes are not included in the Croton et al. (2006) semi-analytic model used here (most semi-analytic models ignore such additional effects to keep the models relatively simple). Their inclusion would typically redden the color of the satellite further with time, worsening an effect that is already too efficient in the current model. Our work indicates that current prescriptions for satellite infall and its consequent effect on star formation may be too simplistic. However, it also highlights the utility of color-dependent clustering measurements in constraining such models.

## 6. SUMMARY AND DISCUSSION

In this paper we use volume-limited subsamples of the DEEP2 Galaxy Redshift Survey data to measure the color and luminosity dependence of galaxy clustering at  $z \sim 1$ . We split the sample into blue, star-forming galaxies and red, nonstar-forming galaxies using the observed color bimodality in  $(U - B)$ . We further subdivide each sample into luminosity and finer color bins.

In this section we first summarize our main results and then discuss their implications. Our main findings are:

- Red galaxies are much more strongly clustered than blue galaxies at  $z \sim 1$ , with a relative bias that is roughly as high as is found locally ( $b_{\text{red}}/b_{\text{blue}} \sim 1.4 - 1.6$ ). This implies that, for relatively bright galaxies, the color-density relation was as strongly in place 8 Gyr ago as it is observed to be today.
- The comoving clustering amplitudes that we measure for both blue and red galaxies are only slightly (10-20%) lower than what is found locally. The measured values are somewhat higher than those in previous DEEP2 and VVDS results (Coil et al. 2004b; Meneux et al. 2006), though generally within  $2\sigma$ .
- We find no statistically-significant dependence of galaxy clustering on luminosity for either red or blue galaxies, within the luminosity range that we probe. Additionally, within the red sequence there is no dependence of clustering on color, while within the blue cloud there is a strong dependence on color. The color dependence and lack of luminosity dependence for both red and blue that we find is consistent with previous results at  $z = 0.1$ , for the luminosity range probed here.
- The stronger dependence of clustering on luminosity found for all galaxies in the DEEP2 sample (Coil et al. 2006a) is likely due in part to the changing fraction of red versus blue galaxies as a function of luminosity, as we do not find as strong of a luminosity dependence here within either the red or blue galaxy populations independently.
- The brightest blue galaxies have a significant rise in their correlation function on small scales ( $r_p < 0.2 h^{-1}$  Mpc), which likely reflects a lower satellite fraction compared to fainter blue galaxies; i.e., bright blue galaxies are more likely to be central galaxies within their parent dark matter halos.
- The correlation between color and clustering within the blue cloud is likely a reflection of a correlation between stellar mass and halo mass. The redder galaxies in the blue cloud have higher stellar masses (see Figure 8 of Cooper et al. 2007b) and are significantly more clustered than the bluer galaxies, which implies that they are in more massive dark matter halos.
- Red galaxies show strong ‘fingers of god’ at  $z \sim 1$ , indicating that they lie in virialized overdensities such as groups and clusters. Blue galaxies show smaller ‘fingers of god’.

- Both blue and red galaxies show a flattening of  $\xi(r_p, \pi)$  on large scales due to coherent infall of galaxies onto structures that are still collapsing (the Kaiser effect).
- The projected correlation functions of brighter samples near  $L^*$  show deviations from a power law on small scales, within the one-halo regime. The deviations are more pronounced for blue galaxies than for red galaxies.
- The red-blue cross-correlation function is consistent with the geometric mean of the auto-correlation functions of blue and red galaxies separately. There is a marginal trend on small scales for the cross-correlation to lie below the geometric mean. Such a feature, if real, would indicate a lack of blue galaxies near red galaxies. This could reflect a suppression of star formation in the centers of overdensities, such as groups, which are dominated by red galaxies at  $z \sim 1$  as seen in the group-galaxy cross-correlation function (Coil et al. 2006b).
- Green galaxies in the valley of the observed color bimodality display a similar large-scale clustering strength as red galaxies, but show a small-scale clustering amplitude and infall kinematics akin to blue galaxies. The green galaxy population does not have strong ‘fingers of god’ but does show coherent infall on large scales, and the correlation function has a similar slope to the blue galaxy population. Green galaxies thus appear to be at the edges, but not in the centers, of the same overdensities as red galaxies. This is consistent with green galaxies being transition objects moving from the blue cloud to the red sequence and supports a picture of quenching happening preferentially on the outskirts of overdensities at  $z \sim 1$  on scales  $r_p \sim 0.5 - 2 h^{-1}$  Mpc.
- We provide a direct test of environment and clustering statistics, comparing the relative bias as a function of color using a local galaxy overdensity estimator with the two-point correlation function results, and find good agreement between the two.
- Comparing with the semi-analytic galaxy evolution model of Croton et al. (2006), we find that red model galaxies are significantly more clustered than the DEEP2 galaxies, and that in the model the clustering strength of blue galaxies is too low, especially on small scales ( $r_p < 0.5 h^{-1}$  Mpc). These discrepancies are likely due to galaxies being quenched too efficiently in the model; i.e., star formation is shut down in satellite galaxies too quickly.
- These results all rely on precise, robust, spectroscopic redshifts. The DEEP2 rms redshift errors (determined from repeated observations) are  $< 35$  km s $^{-1}$ , which is unprecedented at  $z \sim 1$  and makes the  $\xi(r_p, \pi)$  analyses presented here possible.

From the observed bias of the main red and blue galaxy samples we can infer the minimum dark matter mass for halos that host these galaxies. Un-

der the assumption that all galaxies are central galaxies and not satellites (i.e., one galaxy per dark matter halo), the large scale bias of the galaxy population can be matched to the bias of dark matter halos using the formulae from e.g., Mo & White (1996) or Sheth, Mo & Tormen (2001). However, we know that not all of the DEEP2 galaxies are central galaxies (Gerke et al. 2005; Conroy, Wechsler, & Kravtsov 2006; Zheng, Coil, & Zehavi 2007), and to obtain a more precise estimate of the minimum dark matter halo mass we use the results presented in the Appendix of Zheng, Coil, & Zehavi (2007), which take into account the inferred satellite fraction from HOD modeling of the DEEP2 luminosity-dependent clustering results (Coil et al. 2006a). At  $z = 0.9$ , the observed bias and number densities of the main red and blue galaxy samples (with  $M_B \leq -20.0$ ) imply minimum dark matter halo masses of  $M_{min} \sim 2 \times 10^{12} h^{-1} M_\odot$  for red galaxies and  $M_{min} \sim 5 \times 10^{11} h^{-1} M_\odot$  for blue galaxies. However, the halo occupation of red and blue galaxies is likely complicated enough to warrant a full HOD model, which we defer to a future paper (see, e.g., van den Bosch, Yang, & Mo 2003; Collister & Lahav 2005; Zehavi et al. 2005, for modeling of local red and blue samples).

The different slopes measured for the clustering of red and blue galaxies would pose a potential difficulty in terms of understanding how red and blue galaxies populate dark matter halos, if the slopes were different on large scales ( $r_p \gtrsim 2 h^{-1}$  Mpc). On these scales the halo bias is linear, in that there is an amplitude offset between  $\xi(r)$  for halos of different mass, but no difference in the slope (e.g., van den Bosch, Yang, & Mo 2003; Conroy, Wechsler, & Kravtsov 2006). We do not have a large enough survey here to claim a significant difference in the slope on scales  $r_p \gtrsim 2 h^{-1}$  Mpc, though the upper left panel of Figure 4 does suggest such a difference.

It has been previously established that the number density of galaxies on the red sequence has increased since  $z = 1$  (Bell et al. 2004; Faber et al. 2007; Brown et al. 2007). It is thought that these galaxies likely migrated from the blue cloud to the red sequence as their star formation was quenched. Using the observed clustering of red and blue galaxies at  $z \sim 1$ , one can predict what their clustering strength should be at  $z \sim 0$ , for a given cosmology and assuming no merging of galaxies, by using the continuity equation and the expected growth of perturbations (Tegmark & Peebles 1998). This leads to larger predicted clustering amplitudes than is observed for local  $L^*$  red and blue galaxies; the main red and blue samples used here (both of which have  $L \sim L^*$  at  $z = 0.9$ ) would have clustering scale-lengths of  $r_0 = 6.5 h^{-1}$  Mpc and  $r_0 = 5.5 h^{-1}$  Mpc, respectively, at  $z = 0$ . The fact that local clustering measurements at  $L^*$  are lower than these predictions, especially for blue galaxies, lends credence to the idea that blue galaxies have migrated to the red sequence and less clustered blue galaxies have joined the blue cloud since  $z = 1$ .

The color and luminosity dependence of clustering at  $z = 1$  can illuminate *which* blue galaxies likely become red between  $z = 1$  and  $z = 0$ . The fact that the relative bias between red and blue galaxies is as high at  $z \sim 1$  as  $z \sim 0$  indicates that blue galaxies have to be turning red *in a density-dependent way*, in that the more clus-

tered of the blue galaxies must become red. The bias for any galaxy population should tend towards unity with time (Fry 1996) and linear growth theory would predict that the relative bias of our red and blue samples should decrease by 8% to  $z = 0.1$ . Observationally, however, it appears that the relative bias between red and blue galaxies has either remained constant since  $z \sim 1$  or increased. This therefore implies that the most clustered blue galaxies must be turning red to boost the clustering of red galaxies relative to blue galaxies and to counteract the effect of the relative bias decreasing. It is the most clustered of the blue galaxies at  $z = 1$  that are likely to be as clustered as red galaxies by  $z = 0$ , and our results here indicate that the reddest of the blue galaxies and the green galaxies are the most likely candidates for having their star formation quenched by  $z = 0$ , based on their clustering properties.

The luminosity dependence of clustering at  $z \sim 1$  can be explained as being almost entirely due to the relationship between luminosity and halo mass, as shown by Conroy, Wechsler, & Kravtsov (2006) who use a simple one-to-one relation between halo mass and light to obtain the same luminosity- and scale-dependence of clustering in an N-body simulation as we find in DEEP2. The tight relation between halo mass and galaxy light is confirmed by Zheng, Coil, & Zehavi (2007), who fit HOD models to the DEEP2 luminosity dependent clustering results. However, the color dependence of clustering seen here can not entirely be halo-mass dependent, as the clustering as a function of color does not match the results of Conroy, Wechsler, & Kravtsov (2006), where the galaxies have been ranked by luminosity, which is equivalent to halo mass; i.e., the trends seen with color in the data do not match the trends found with luminosity or halo mass in the model. This implies that there is a wider range in the  $M_{\text{halo}}/L$  ratio of galaxies at a given color than at a given luminosity. To constrain galaxy evolution physics it may therefore be more informative to study samples divided by color rather than luminosity, as more galaxy physics is apparently needed to interpret the color dependence of galaxy clustering. The lack of a stronger luminosity dependence for the separate red and blue galaxy samples shown here makes the results of Conroy, Wechsler, & Kravtsov (2006) more surprising, as it is not clear why  $M_B$  luminosity for all galaxies should be so tightly correlated with halo mass. It may be that the relative mix of red and blue galaxies as a function of luminosity helps to create a stronger relation with luminosity for all galaxies and is more tightly correlated with halo mass than the luminosity itself.

As noted in previous papers on the color-density relation in the DEEP2 sample (Gerke et al. 2007; Cooper et al. 2006), the observed color-density relation at  $z \sim 1$  can not be the result of cluster-specific physics as only a few percent of DEEP2 galaxies are in massive clusters. The color dependence of clustering must be dominated by either processes that operate in a group environment or intrinsic processes that depend on the age, stellar mass or halo mass of a galaxy. Processes that occur when a galaxy is accreted into a larger halo, becoming a satellite galaxy, may *contribute* to the observed color-density relation but do not *dominate* it, as most DEEP2 galaxies are not satellite galaxies (Gerke et al. 2005; Zheng, Coil, & Zehavi 2007). What star-formation

quenching processes may be at work in groups? There are more galaxy mergers in groups than in clusters, such that mergers may play an important role in shutting off star formation in group galaxies. There is less hot ambient gas in groups than in clusters; it is not clear whether the density of the intragroup gas is high enough to strip gas from infalling satellite galaxies, except near the core of the group. Apparently not all satellite galaxies are red, as is seen in the clustering results; this implies that there is a non-negligible timescale for quenching star formation in satellite galaxies.

DEEP2 galaxies in groups at  $z \sim 1$  have a clustering scale-length of  $r_0 = 4.97 \pm 0.25 h^{-1}$  Mpc and a slope of  $\gamma = 2.15 \pm 0.06$  (Coil et al. 2006b), similar to red galaxies as measured here. Galaxies in the field at  $z \sim 1$  have a slope of  $\gamma = 1.70 \pm 0.13$ , similar to blue galaxies, but with a lower correlation length,  $r_0 = 2.54 \pm 0.25 h^{-1}$  Mpc. The cross-correlation of red galaxies and groups is higher than that of blue galaxies and groups (Coil et al. 2006b), which also indicates that red galaxies are more likely to be in groups. However, the picture is not as simple as all red galaxies being in groups and blue galaxies being in the field: blue galaxies have some fingers of god on small scales, indicating that at least some are in virialized overdensities, and the brighter blue galaxies show a rise in the correlation function on small scales, which is probably due to a lower satellite fraction for the brighter blue samples. These galaxies are likely the central galaxies in groups at  $z = 1$ , and may migrate to the red sequence by  $z \sim 0$ . The scale at which the one-halo term rise occurs for these samples is small,  $r_p \sim 0.3 h^{-1}$  Mpc (as seen in Figure 10), and indicates again that these galaxies are likely to be in the centers of the groups they reside in. Additionally,  $\sim 5 - 10\%$  of DEEP2 galaxies in underdense regions are red (Cooper et al. 2007a).

The green galaxy population, which lies near the minimum in the observed color bimodality, appears to be, at least in part, a distinct population and is not a simple mix of red and blue galaxies. Though the green population can include the tail of each of the blue and red distributions, it also contains transitional objects, likely moving from the blue cloud to the red sequence. The green galaxies have different clustering characteristics than either the red or blue galaxies as a whole. On large scales ( $r_p > 1 h^{-1}$  Mpc) the green galaxies are as clustered as red galaxies of the same luminosity, implying that they reside in the same relatively massive halos as red galaxies. On small scales, however, the clustering amplitude is similar to that of blue galaxies, which likely reflects a lower radial concentration for green galaxies compared to red galaxies. The general picture that emerges is one in which star formation quenching is occurring primarily at the edges of overdensities as galaxies fall in, turning blue galaxies green around the edges of groups.

We have identified that the scale at which this transition from red to blue occurs at  $z \sim 1$  is  $0.5 h^{-1}$  Mpc  $< r_p < 2 h^{-1}$  Mpc. This scale is just larger than the transition scale between the one-halo and two-halo terms at  $z \sim 1$ , which is shown by Zheng, Coil, & Zehavi (2007) (see their Fig. 1) to be  $\sim 0.5 h^{-1}$  Mpc for all galaxies and by Coil et al. (2006b) (see their Fig. 8) to be  $\sim 1.0 h^{-1}$  Mpc for galaxies in groups. This transition scale for green galaxies is therefore similar to or just larger than the largest halos, which indicates that it is occurring at



$\sim 1 - 2$  virial radii, on the edges of large halos. This conclusion lends support to the idea that the mechanism which shuts off star formation in these galaxies is not happening at the centers of massive halos, but on the outskirts.

The comparison to semi-analytic galaxy formation models demonstrates vividly the utility of using correlation statistics to test theoretical models, and the need to test them at intermediate redshift, not just locally. It is also likely that currently popular models that have a simple halo threshold mass for quenching star formation in galaxies will suffer similar problems as the model shown here. We urge theorists to use these data to constrain their models.

We thank Charlie Conroy, Daniel Eisenstein, Jeremy Tinker, Frank van den Bosch, Christopher Willmer and Zheng Zheng for useful discussions and comments on this paper. ALC and NP are supported by NASA through Hubble Fellowship grants HF-01182.01-A and HST-HF-

01200, respectively, awarded by the Space Telescope Science Institute, which is operated by the Association of Universities for Research in Astronomy, Inc., for NASA, under contract NAS 5-26555. The DEIMOS spectrograph was funded by a grant from CARA (Keck Observatory), an NSF Facilities and Infrastructure grant (AST92-2540), the Center for Particle Astrophysics and by gifts from Sun Microsystems and the Quantum Corporation. The data presented herein were obtained at the W.M. Keck Observatory, which is operated as a scientific partnership among the California Institute of Technology, the University of California and the National Aeronautics and Space Administration. The Observatory was made possible by the generous financial support of the W.M. Keck Foundation. The DEEP2 team and Keck Observatory acknowledge the very significant cultural role and reverence that the summit of Mauna Kea has always had within the indigenous Hawaiian community and appreciate the opportunity to conduct observations from this mountain.

#### REFERENCES

- Abazajian, K., et al. 2005, *ApJ*, 625, 613  
 Barton, E. J., Geller, M. J., & Kenyon, S. J. 2000, *ApJ*, 530, 660  
 Bell, E. F., et al. 2004, *ApJ*, 608, 752  
 Berlind, A. A., et al. 2005, *ApJ*, 629, 625  
 Berlind, A. A., & Weinberg, D. H. 2002, *ApJ*, 575, 587  
 Blanton, M. R., et al. 2003a, *ApJ*, 594, 186  
 Blanton, M. R., et al. 2003b, *ApJ*, 592, 819  
 Brown, M. J. I., et al. 2003, *ApJ*, 597, 225  
 Brown, M. J. I., et al. 2007, *ApJ*, 654, 858  
 Budavari, T., et al. 2003, *ApJ*, 595, 59  
 Bundy, K., et al. 2006, *ApJ*, 651, 120  
 Byrd, G., & Valtonen, M. 1990, *ApJ*, 350, 89  
 Carlberg, R. G., et al. 1997, *ApJ*, 484, 538  
 Carlberg, R. G., et al. 2001, *ApJ*, 563, 736  
 Cen, R., & Ostriker, J. P. 2000, *ApJ*, 538, 83  
 Coil, A. L., et al. 2004a, *ApJ*, 617, 765  
 Coil, A. L., et al. 2004b, *ApJ*, 609, 525  
 Coil, A. L., et al. 2006a, *ApJ*, 644, 671  
 Coil, A. L., et al. 2006b, *ApJ*, 638, 668  
 Collister, A. A., & Lahav, O. 2005, *MNRAS*, 361, 415  
 Conroy, C., Wechsler, R. H., & Kravtsov, A. V. 2006, *ApJ*, 647, 201  
 Cooper, M. C., et al. 2006, *MNRAS*, 370, 198  
 Cooper, M. C., et al. 2007a, Accepted to *MNRAS*, astro-ph/0607512  
 Cooper, M. C., et al. 2007b, ArXiv e-prints, 706  
 Croton, D. J., et al. 2006, *MNRAS*, 365, 11  
 Cucciati, O., et al. 2006, *A&A*, 458, 39  
 Davis, M., et al. 2003, *Proc. SPIE*, 4834, 161 (astro-ph 0209419)  
 Davis, M., et al. 2007, *ApJ*, 660, L1  
 Davis, M., & Geller, M. J. 1976, *ApJ*, 208, 13  
 Davis, M., & Peebles, P. J. E. 1977, *ApJS*, 34, 425  
 Davis, M., & Peebles, P. J. E. 1983, *ApJ*, 267, 465  
 Davis, M., Gerke, B. F., & Newman, J. A. 2005, In Proceedings of "Observing Dark Energy: NOAO Workshop", Mar 18-20, 2004  
 Diaferio, A., & Geller, M. J. 1996, *ApJ*, 467, 19  
 Dressler, A. 1980, *ApJ*, 236, 351  
 Eisenstein, D. J., et al. 2005, *ApJ*, 633, 560–574  
 Faber, S., et al. 2003, *Proc. SPIE*, 4841, 1657  
 Faber, S. M., et al. 2007, Accepted to *ApJ*, astro-ph/0506044  
 Firth, A. E., et al. 2002, *MNRAS*, 332, 617  
 Fisher, K. B., et al. 1994, *MNRAS*, 267, 927  
 Fry, J. N. 1996, *ApJ*, 461, L65  
 Gerke, B. F., et al. 2005, *ApJ*, 625, 6  
 Gerke, B. F., et al. 2007, *MNRAS*, 376, 1425  
 Gunn, J. E., & Gott, J. R. I. 1972, *ApJ*, 176, 1  
 Hamilton, A. J. S. 1992, *ApJ*, 385, L5  
 Hamilton, A. J. S. 1993, *ApJ*, 417, 19  
 Hawkins, E., et al. 2003, *MNRAS*, 346, 78  
 Heinis, S., et al. 2007, ArXiv e-prints, 706  
 Hermit, S., et al. 1996, *MNRAS*, 283, 709  
 Hoekstra, H., et al. 2002, *ApJ*, 577, 604  
 Hogg, D. W., et al. 2003, *ApJ*, 585, L5  
 Hogg, D. W., et al. 2004, *ApJ*, 601, L29  
 Kaiser, N. 1987, *MNRAS*, 227, 1  
 Kauffmann, G., et al. 2003, *MNRAS*, 341, 54  
 Kerscher, M., Szapudi, I., & Szalay, A. S. 2000, *ApJ*, 535, L13  
 Kitzbichler, M. G., & White, S. D. M. 2007, *MNRAS*, 376, 2  
 Kravtsov, A. V., et al. 2004, *ApJ*, 609, 35  
 Landy, S. D., & Szalay, A. S. 1993, *ApJ*, 412, 64  
 Le Fèvre, O., et al. 2005, *A&A*, 439, 845  
 Lee, K.-S., et al. 2006, *ApJ*, 642, 63  
 Li, C., et al. 2006a, *MNRAS*, 368, 21  
 Li, C., et al. 2006b, *MNRAS*, 368, 37  
 Loveday, J., Maddox, S. J., Efstathiou, G., & Peterson, B. A. 1995, *ApJ*, 442, 457  
 Madgwick, D. S., et al. 2002, *MNRAS*, 333, 133  
 Madgwick, D. S., et al. 2003a, *MNRAS*, 344, 847  
 Madgwick, D. S., et al. 2003b, *ApJ*, 599, 997  
 Mandelbaum, R., et al. 2006, *MNRAS*, 368, 715  
 Marinoni, C., et al. 2005, *A&A*, 442, 801  
 Meneux, B., et al. 2006, *A&A*, 452, 387  
 Mo, H. J., & White, S. D. M. 1996, *MNRAS*, 282, 347  
 Nandra, K., et al. 2007, *ApJ*, 660, L11  
 Norberg, P., et al. 2002a, *MNRAS*, 336, 907  
 Norberg, P., et al. 2002b, *MNRAS*, 332, 827  
 Ouchi, M., et al. 2005, *ApJ*, 635, L117  
 Padmanabhan, N., White, M., & Eisenstein, D. J. 2007, *MNRAS*, 376, 1702  
 Peacock, J. A., et al. 2001, *Nature*, 410, 169  
 Pearce, F. R., et al. 2001, *MNRAS*, 326, 649  
 Peebles, P. J. E. 1980. *The Large-Scale Structure of the Universe*, Princeton, N.J., Princeton Univ. Press  
 Pheleps, S., Peacock, J. A., Meisenheimer, K., & Wolf, C. 2006, *A&A*, 457, 145  
 Salim, S., et al. 2007, ArXiv e-prints, 704  
 Seljak, U., et al. 2005, *Phys. Rev. D*, 71, 043511  
 Shepherd, C. W., et al. 2001, *ApJ*, 560, 72  
 Sheth, R. K. 1996, *MNRAS*, 279, 1310  
 Sheth, R. K., Mo, H. J., & Tormen, G. 2001, *MNRAS*, 323, 1  
 Simon, P., et al. 2007, *A&A*, 461, 861  
 Smith, R. E., et al. 2003, *MNRAS*, 341, 1311  
 Spergel, D. N., et al. 2003, *ApJS*, 148, 175  
 Springel, V., et al. 2005, *Nature*, 435, 629  
 Strateva, I., et al. 2001, *AJ*, 122, 1861  
 Swanson, M. E., et al. 2007, Submitted to PRD, astro-ph/0702584  
 Tegmark, M., & Peebles, P. J. E. 1998, *ApJ*, 500, L79  
 van den Bosch, F. C., et al. 2007, *MNRAS*, 376, 841  
 van den Bosch, F. C., Yang, X., & Mo, H. J. 2003, *MNRAS*, 340, 771

- Verde, L., et al. 2002, MNRAS, 335, 432  
Wang, Y., et al. 2007, ApJ, 664, 608  
Weinberg, D. H., Davé, R., Katz, N., & Hernquist, L. 2004, ApJ, 601, 1  
Weiner, B. J., et al. 2007, ApJ, 660, L39  
Weinmann, S. M., et al. 2006a, MNRAS, 372, 1161  
Weinmann, S. M., van den Bosch, F. C., Yang, X., & Mo, H. J. 2006b, MNRAS, 366, 2  
Willmer, C., et al. 2006, ApJ, 647, 853  
Willmer, C. N. A., da Costa, L. N., & Pellegrini, P. S. 1998, AJ, 115, 869  
Yan, R., et al. 2006, ApJ, 648, 281  
Yan, R., Madgwick, D. S., & White, M. 2003, ApJ, 598, 848  
Yan, R., White, M., & Coil, A. L. 2004, ApJ, 607, 739  
Yang, X., Mo, H. J., Jing, Y. P., & van den Bosch, F. C. 2005, MNRAS, 358, 217  
Zehavi, I., et al. 2002, ApJ, 571, 172  
Zehavi, I., et al. 2004, ApJ, 608, 16  
Zehavi, I., et al. 2005, ApJ, 630, 1  
Zheng, Z., Coil, A., & Zehavi, I. 2007, Accepted to ApJ, astro-ph/0703457

TABLE 1  
PUBLISHED COLOR CLUSTERING RESULTS

	mean $z$	blue $r_0$	blue $\gamma$	red $r_0$	red $\gamma$	relative bias	M range
Norberg et al. 2002	0.1	$4.45 \pm 0.47$	$1.76 \pm 0.09$	$5.71 \pm 0.57$	$1.87 \pm 0.09$	–	$-20 < M_{bJ} < -19$
Madgwick et al. 2003	0.1	$3.67 \pm 0.30$	$1.60 \pm 0.04$	$6.10 \pm 0.34$	$1.95 \pm 0.03$	$1.45 \pm 0.14$	$\sim M^*$
Budavari et al. 2003	0.2	$\sim 4.5-6.0$	$\sim 1.67 \pm 0.10$	$\sim 6.3 - 6.6 \pm 0.20$	$2.0 \pm 0.5$	–	$-20 > M_{r^*} > -21$
Zehavi et al. 2004	0.1	$3.63 \pm 0.16$	$1.69 \pm 0.04$	$5.67 \pm 0.37$	$2.08 \pm 0.05$	$\sim 1.6$	$-20 < M_r < -19$
Coil et al. 2004	0.8	$2.81 \pm 0.48$	$1.52 \pm 0.06$	$4.32 \pm 0.73$	$1.84 \pm 0.07$	$1.41 \pm 0.10$	
Meneux et al. 2006	0.8	$2.18 \pm 0.30$	$1.40 \pm 0.14$	$3.78 \pm 0.7$	$1.87 \pm 0.25$	$1.45 \pm 0.27$	

TABLE 2  
DEEP2 GALAXY SAMPLES

Sample	No. of galaxies	$n$ ( $h^3 Mpc^{-3}$ )	median ( $U - B$ )	$M_B$ range	Median $M_B$	$z$ range	Mean $z$	$r_0$	$\gamma$	Bias <sup>a</sup>	$\sigma_{12}$
Red: -21.0	792	$3.9 \cdot 10^{-4}$	1.22	$\leq -21.0$	-21.38	0.7 – 1.1	0.92	$5.78 \pm 0.87$	$1.89 \pm 0.17$	$1.79 \pm 0.21$	$360 \pm 70$
Red: -20.5	1370	$9.0 \cdot 10^{-4}$	1.21	$\leq -20.5$	-21.03	0.7 – 1.025	0.88	$5.37 \pm 0.27$	$1.94 \pm 0.06$	$1.71 \pm 0.14$	$500 \pm 50$
Red: -20.0 (main)	1474	$1.6 \cdot 10^{-3}$	1.21	$\leq -20.0$	-20.70	0.7 – 0.925	0.82	$5.25 \pm 0.26$	$2.06 \pm 0.04$	$1.65 \pm 0.15$	$530 \pm 50$
Red: -19.5	1032	$2.4 \cdot 10^{-3}$	1.20	$\leq -19.5$	-20.46	0.7 – 0.825	0.77	$5.04 \pm 0.40$	$2.06 \pm 0.12$	$1.55 \pm 0.15$	$490 \pm 40$
Blue: -21.0	1424	$6.1 \cdot 10^{-4}$	0.81	$\leq -21.0$	-21.28	0.7 – 1.2	1.00	$4.27 \pm 0.43$	$1.75 \pm 0.13$	$1.39 \pm 0.16$	$250 \pm 50$
Blue: -20.5	3747	$1.6 \cdot 10^{-3}$	0.77	$\leq -20.5$	-20.89	0.7 – 1.2	0.99	$3.86 \pm 0.15$	$1.77 \pm 0.05$	$1.30 \pm 0.07$	$360 \pm 30$
Blue: -20.0 (main)	4808	$3.5 \cdot 10^{-3}$	0.74	$\leq -20.0$	-20.48	0.7 – 1.05	0.90	$3.87 \pm 0.12$	$1.64 \pm 0.05$	$1.28 \pm 0.04$	$240 \pm 20$
Blue: -19.5	4018	$6.3 \cdot 10^{-3}$	0.68	$\leq -19.5$	-20.10	0.7 – 0.9	0.81	$3.58 \pm 0.25$	$1.66 \pm 0.07$	$1.24 \pm 0.08$	$270 \pm 20$
Red: Redder	731	$7.9 \cdot 10^{-4}$	1.27	$\leq -20.0$	-20.66	0.7 – 0.925	0.81	$5.12 \pm 0.51$	$2.17 \pm 0.07$	$1.60 \pm 0.21$	$740 \pm 180$
Red: Bluer	743	$8.1 \cdot 10^{-4}$	1.12	$\leq -20.0$	-20.61	0.7 – 0.925	0.82	$5.18 \pm 0.57$	$2.13 \pm 0.09$	$1.61 \pm 0.22$	$740 \pm 190$
Green	997	$7.7 \cdot 10^{-4}$	1.00	$\leq -20.0$	-20.65	0.7 – 1.0	0.87	$5.17 \pm 0.42$	$1.59 \pm 0.08$	$1.65 \pm 0.26$	$490 \pm 110$
Blue: Redder	1407	$1.3 \cdot 10^{-3}$	0.88	$\leq -20.0$	-20.65	0.7 – 1.0	0.88	$4.49 \pm 0.35$	$1.64 \pm 0.14$	$1.44 \pm 0.19$	$320 \pm 40$
Blue: Middle	1204	$1.1 \cdot 10^{-3}$	0.72	$\leq -20.0$	-20.44	0.7 – 1.0	0.87	$3.63 \pm 0.18$	$1.84 \pm 0.12$	$1.29 \pm 0.20$	$270 \pm 50$
Blue: Bluer	1214	$1.1 \cdot 10^{-3}$	0.56	$\leq -20.0$	-20.33	0.7 – 1.0	0.86	$3.16 \pm 0.15$	$1.78 \pm 0.14$	$1.11 \pm 0.28$	$260 \pm 70$
MR+SAM Red <sup>b</sup> :	7875	$1.4 \cdot 10^{-3}$	1.14	$\leq -20.0$	-20.40	0.7 – 1.0	0.89	$6.31 \pm 0.25$	$1.91 \pm 0.04$	$1.96 \pm 0.14$	$490 \pm 30$
MR+SAM Blue:	23645	$4.2 \cdot 10^{-3}$	0.65	$\leq -20.0$	-20.43	0.7 – 1.0	0.88	$3.27 \pm 0.07$	$1.50 \pm 0.03$	$1.20 \pm 0.10$	$140 \pm 20$

<sup>a</sup> For a  $\Lambda$ CDM model with  $\sigma_8 = 0.9$ .

<sup>b</sup> MR+SAM: Millenium Run with semi-analytic model

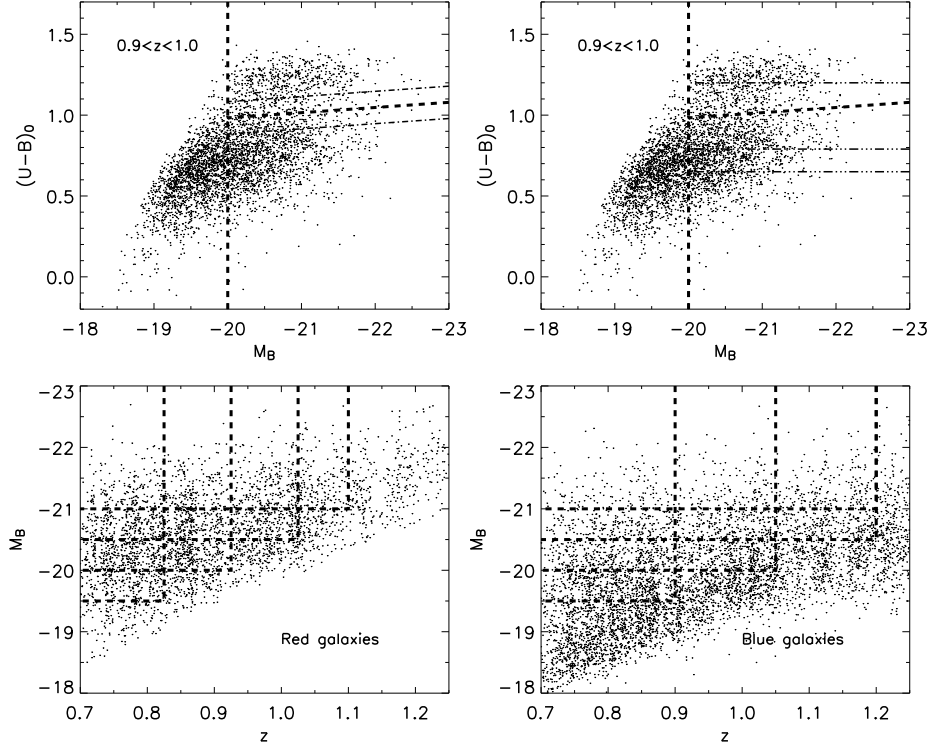


FIG. 1.— Top row: Restframe color-magnitude diagrams for DEEP2 galaxies in the redshift range  $0.7 < z < 1.0$ . The bold vertical dashed line indicates the  $M_B = -20.0$  luminosity cut used for our main color samples, while the tilted and horizontal dashed lines show the various color divisions used to create color subsamples. The left panel shows the cuts for the main red and blue samples (bold dashed lines) and the green sample (thin dashed lines), while the right panel shows the finer color bins used to further divide the main red and blue samples. Bottom row:  $M_B$  versus redshift for red(left) and blue(right) galaxies in the full DEEP2 sample. The magnitude and redshift ranges of the red and blue luminosity samples used here are shown with dashed lines, and properties of each sample are given in Table 2. The blue galaxy sample has been randomly diluted for clarity in this figure.

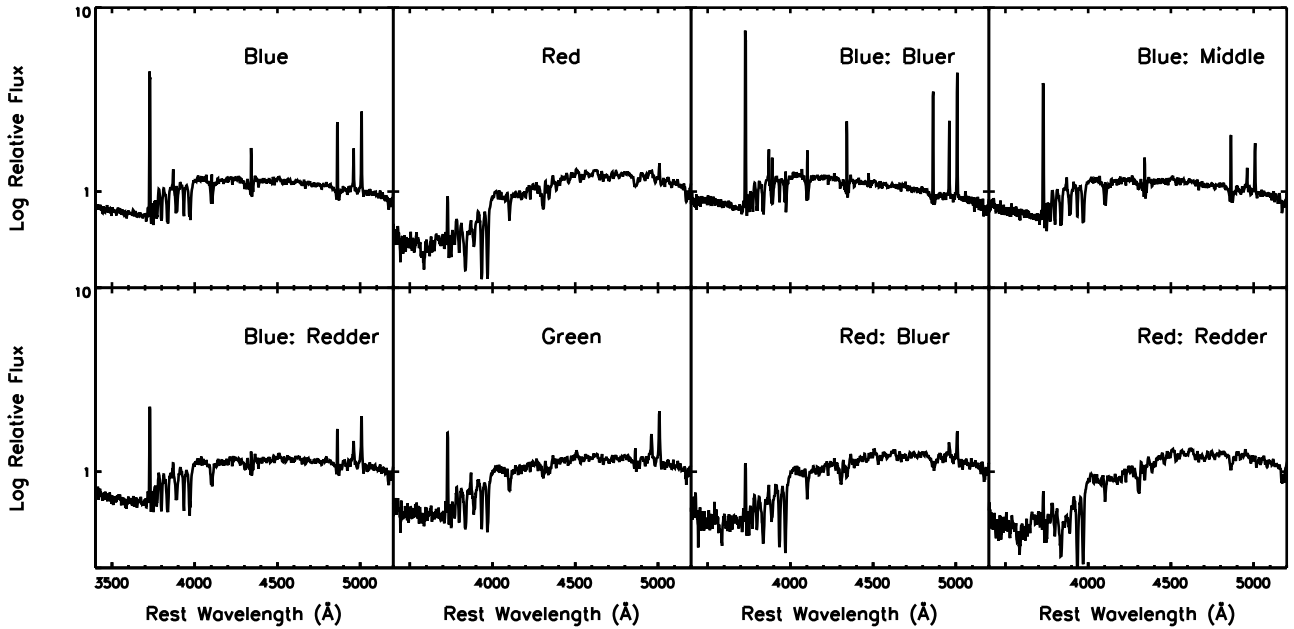


FIG. 2.— Coadded spectra of galaxies in the various color samples used here. The top left panels show average spectra for the main blue and red color samples, while the other panels show spectra for the finer color bins. The correspondence between restframe color and spectral type is clear.

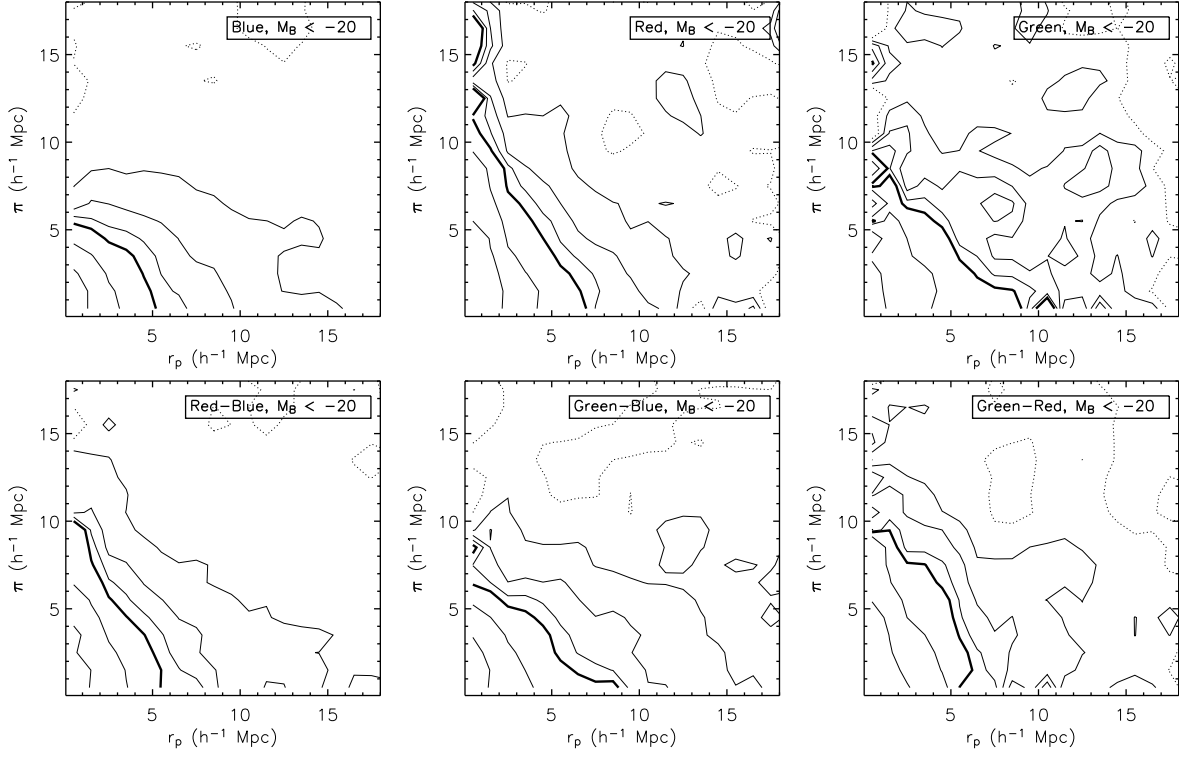


FIG. 3.— Contours of constant correlation strength for the two-dimensional correlation function,  $\xi(r_p, \pi)$ , for the main blue, red and green samples (top row) and various cross-correlation functions (bottom row). A  $1 \times 1 h^{-1}$  Mpc boxcar smoothing has been applied in the figure, though it is not used in calculations. Contours levels are 0.0 (dashed), 0.25, 0.5, 0.75, 1.0 (bold), 2.0 and 5.0.

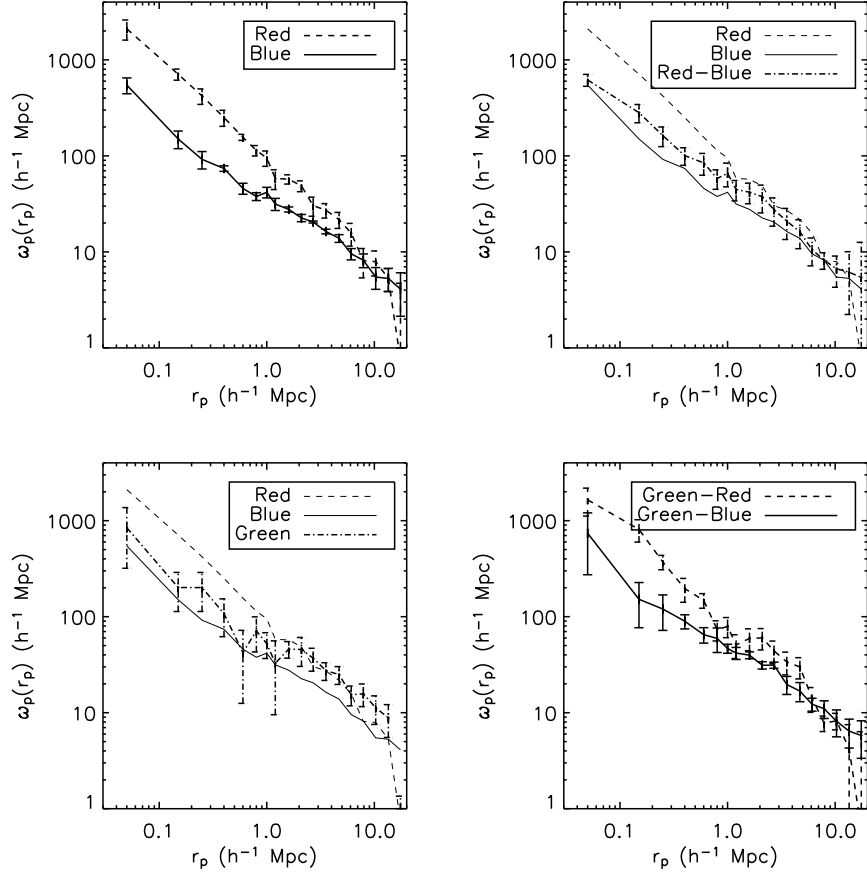


FIG. 4.— The projected correlation function,  $w_p(r_p)$ , for various color samples and cross-correlations. Errors are computed from the variance across the ten pointings on the sky. Corrections have been applied for observational biases due to slitmask effects (see text for details).

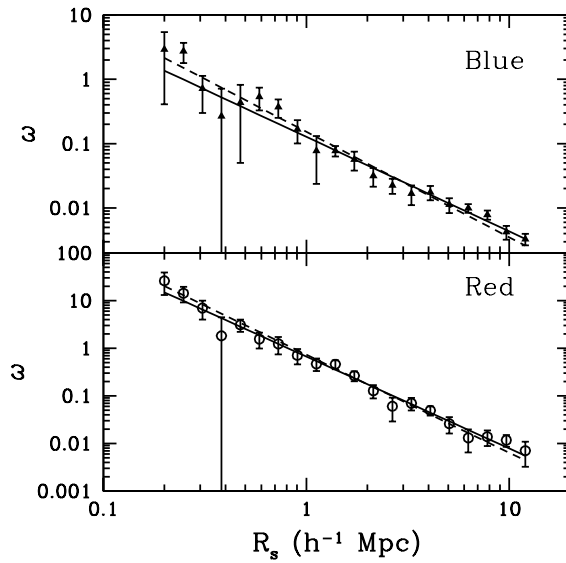


FIG. 5.— The clustering of the main red and blue galaxy samples, as measured by the  $\omega$  estimator of Padmanabhan, White, & Eisenstein (2007) (see §3.3 for details). Note that adjacent points are correlated. The solid line shows the best fit power law to these measurements, while the dashed line shows the result of a power-law fit to the  $w_p(r_p)$  points in Fig. 4. There is good agreement between the two fits, given the measurement errors.

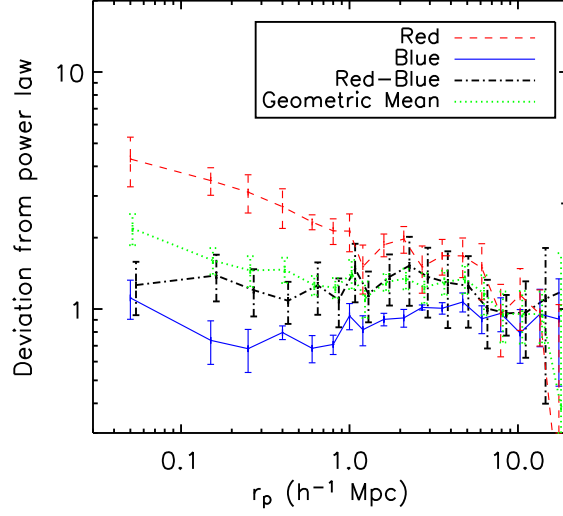


FIG. 6.— Deviations of  $w_p(r_p)$  from a power law with  $r_0 = 4 h^{-1}$  Mpc and  $\gamma = 1.8$  for the main red and blue samples and the red-blue cross-correlation. The cross-correlation is seen to be closer to the blue auto-correlation on small scales, at  $r_p < 1 h^{-1}$  Mpc. The geometric mean of the main red and blue  $w_p(r_p)$  is shown as a dotted line for comparison with the measured cross-correlation function.

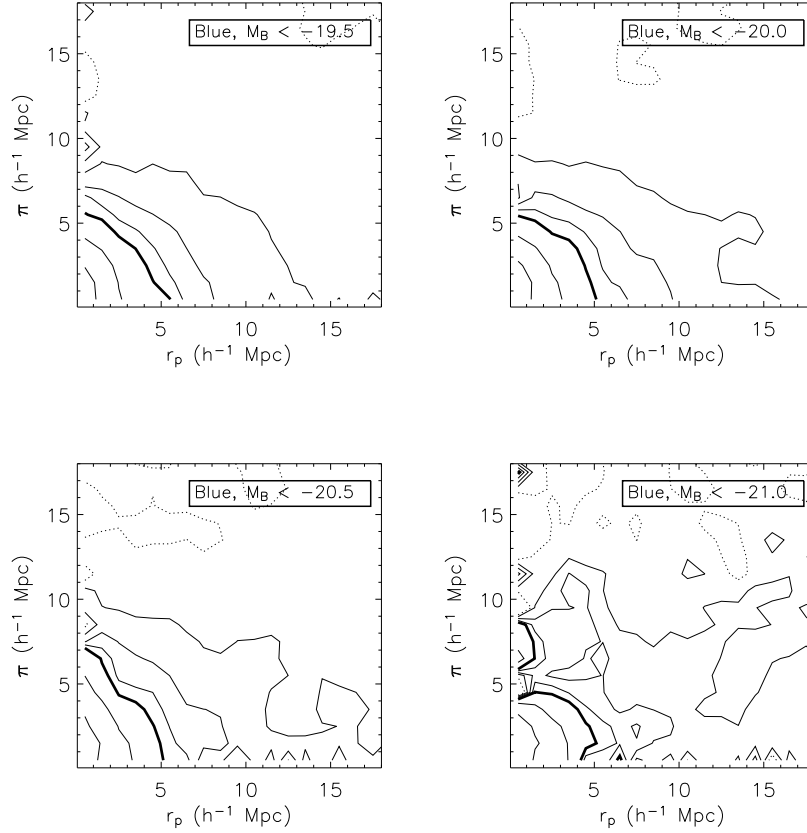


FIG. 7.— Contours of constant correlation strength for the two-dimensional correlation function,  $\xi(r_p, \pi)$ , for the blue luminosity subsamples. A  $1 \times 1 h^{-1}$  Mpc boxcar smoothing has been applied in the figure, though it is not used in calculations. Contour levels are the same as in Figure 3. The strength of the fingers of god on small scales are seen to increase with luminosity in these samples.

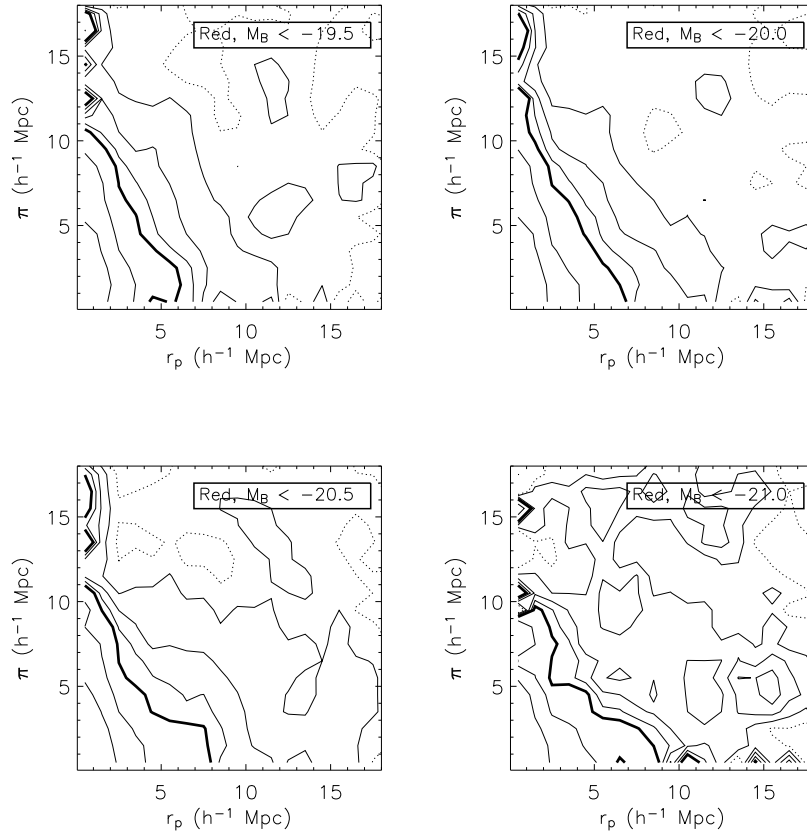


FIG. 8.— Contours of constant correlation strength for the two-dimensional correlation function,  $\xi(r_p, \pi)$ , for the red luminosity subsamples. A  $1 \times 1 h^{-1}$  Mpc boxcar smoothing has been applied in the figure, though it is not used in calculations. Contour levels are the same as in Figure 3. Strong fingers of god are seen in each of the red luminosity samples.



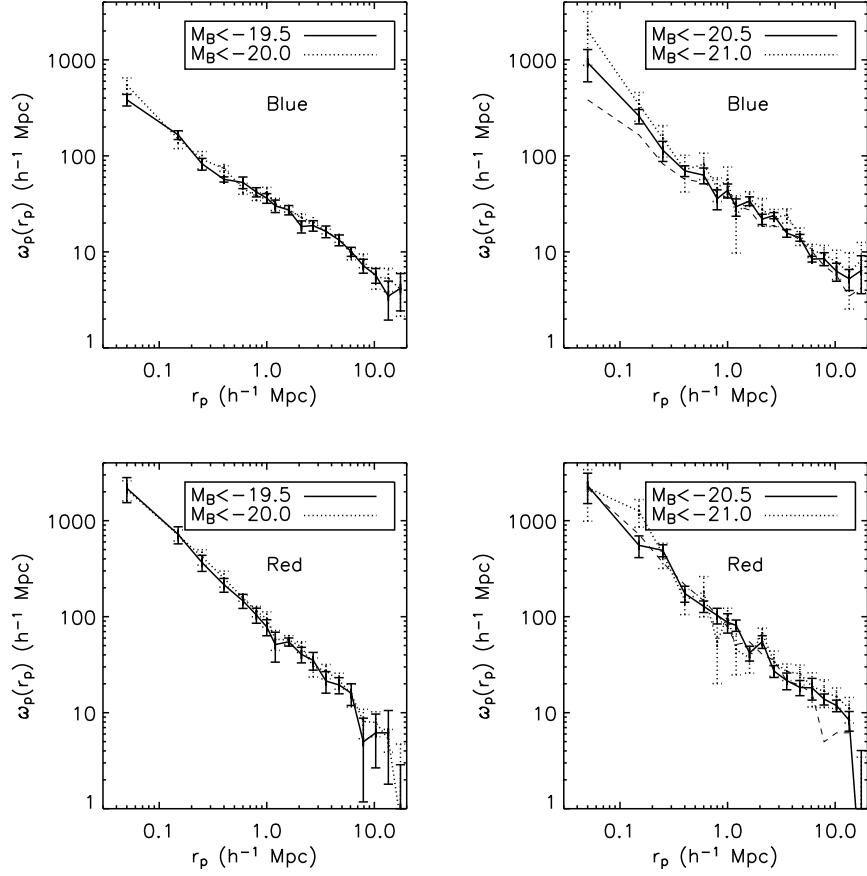


FIG. 9.— The projected correlation function,  $w_p(r_p)$ , for the blue (top) and red (bottom) luminosity subsamples. There is little luminosity dependence seen in the fainter samples (left). Both blue and red galaxies show departures from a power law with a rise in the correlation function on small scales ( $r_p < 0.3 h^{-1}$  Mpc) in the brighter samples with  $M_B < -20.5$  (right). In the right panels the thin dashed line shows the  $M_B < -19.5$  results from the left panel for comparison.

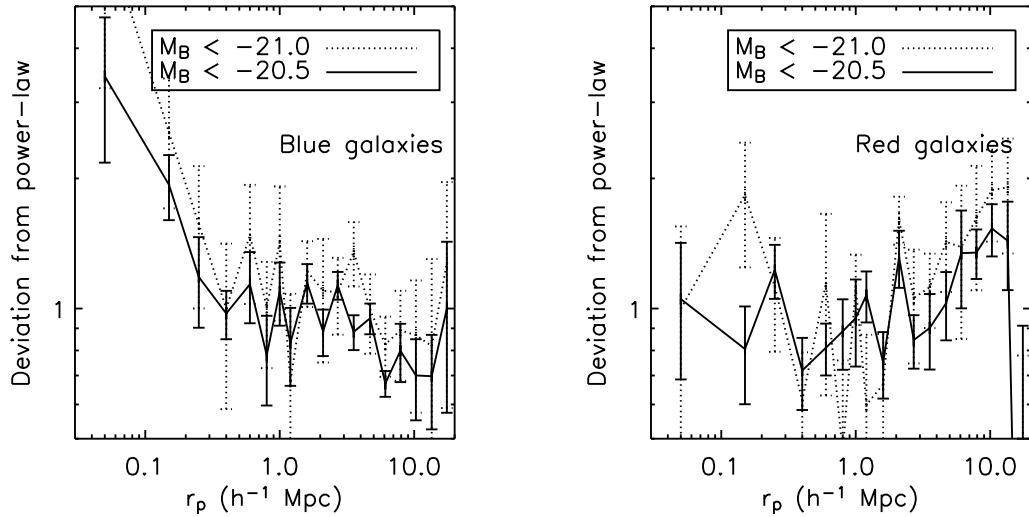


FIG. 10.— Deviations of  $w_p(r_p)$  from the best fit power law for the main blue and red samples for the brighter blue (left) and red (right) luminosity samples. A significant rise is seen on small scales for both blue and red galaxies in the brightest samples.

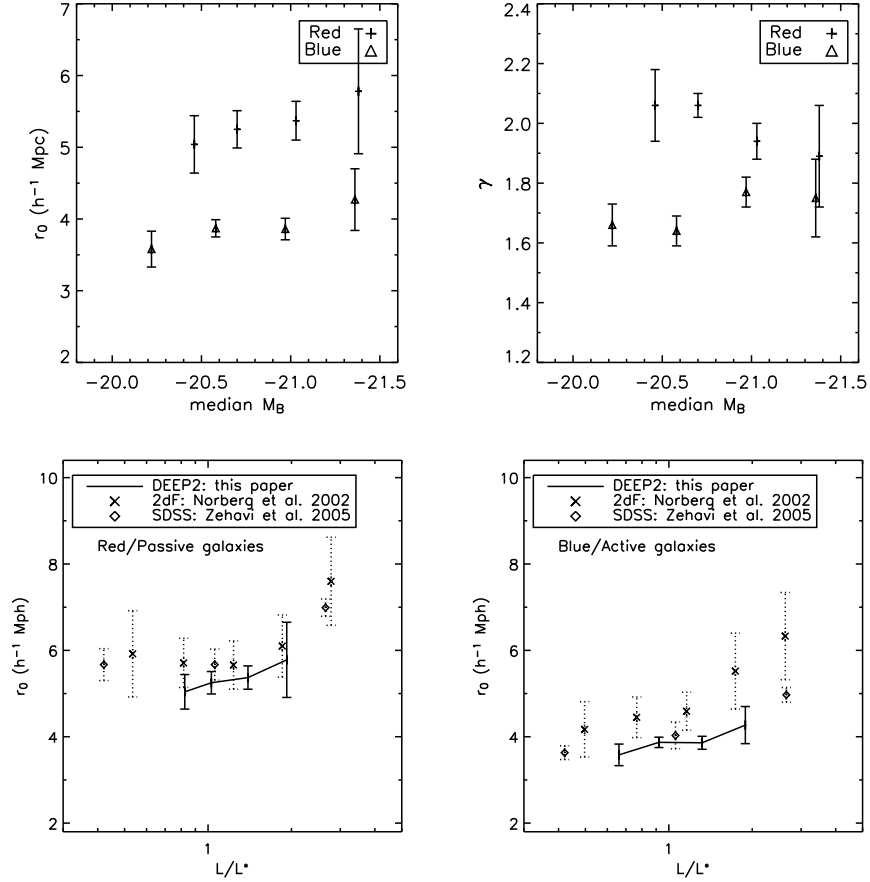


FIG. 11.— The clustering scale-length  $r_0$  (left) and slope  $\gamma$  (right) for DEEP2 galaxies as a function of median absolute  $M_B$  magnitude (top) and  $L/L^*$  (bottom) for both red and blue galaxies. The values of  $r_0$  and  $\gamma$  for each luminosity sample are given in Table 2. Errors are estimated using the variance of power-law fits to jackknife samples. In the lower panels we compare the scale-length for red (left) and blue (right) galaxies found here at  $z \sim 1$  with local results from 2dF (Norberg et al. 2002b) and SDSS (Zehavi et al. 2005).

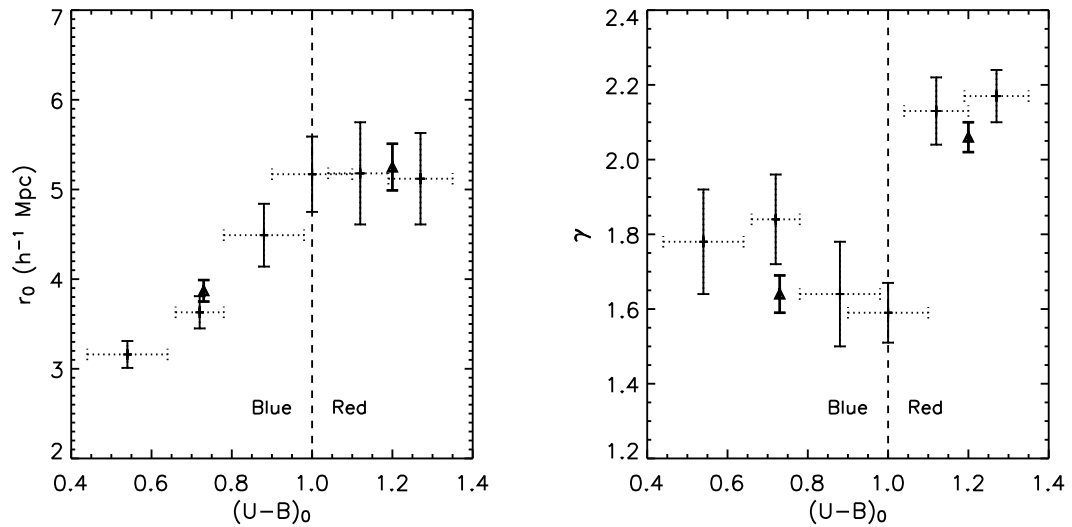


FIG. 12.— The clustering scale-length,  $r_0$  (left), and slope,  $\gamma$  (right), of DEEP2 galaxies as a function of restframe color. The values of  $r_0$  and  $\gamma$  for each color sample are given in Table 2. Errors are estimated using the variance of power-law fits to jackknife samples. Dotted horizontal lines indicate the color range for each point; for clarity the color ranges for the main blue and red samples, shown as triangles, are omitted. The vertical dashed line indicates the approximate location of the minimum in the color bi-modality which separates red and blue galaxies.

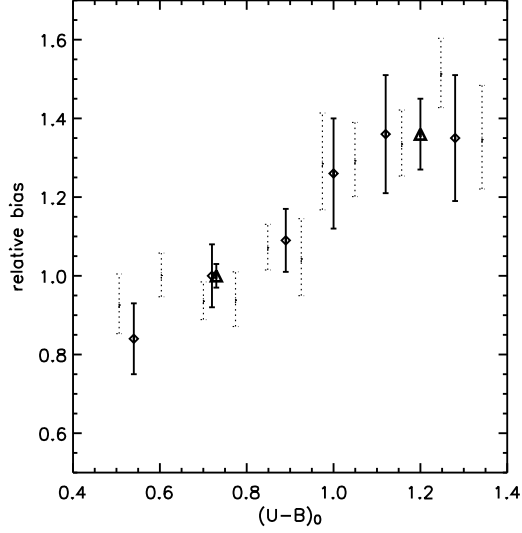


FIG. 13.— The mean relative bias of each of the color samples compared to the main blue sample, averaged on scales  $r_p = 1 - 5 h^{-1}$  Mpc. Triangles show the main red and blue samples and diamonds show the finer color bins. Dotted lines show the relative overdensity as a function of color derived from the  $\delta_3$  environment parameter of Cooper et al. (2006), again normalized to the main blue sample color, which agrees very well with the relative bias measured from the correlation function.

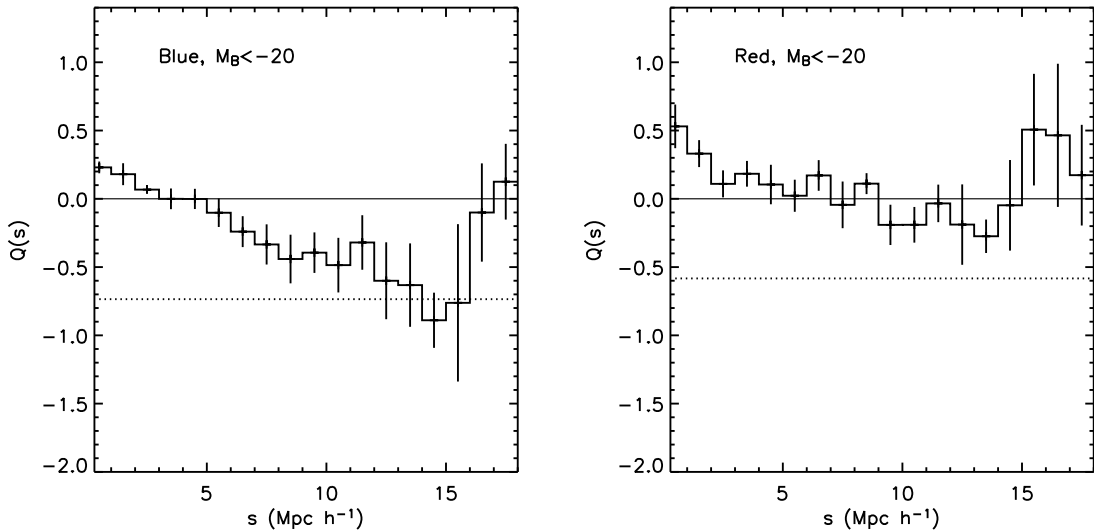


FIG. 14.— The quadrupole-to-monopole ratio, defined as  $Q(s) \equiv \xi_2/(\xi_0 - \xi_0)$ , as a function of scale for the main blue (left) and red (right) samples. Dotted lines show the expectations from linear theory for  $\beta = 0.65$  for blue galaxies and  $\beta = 0.52$  for red galaxies, where  $\beta \equiv \Omega_M^{0.6}/b$  and  $b$  is the linear galaxy bias.

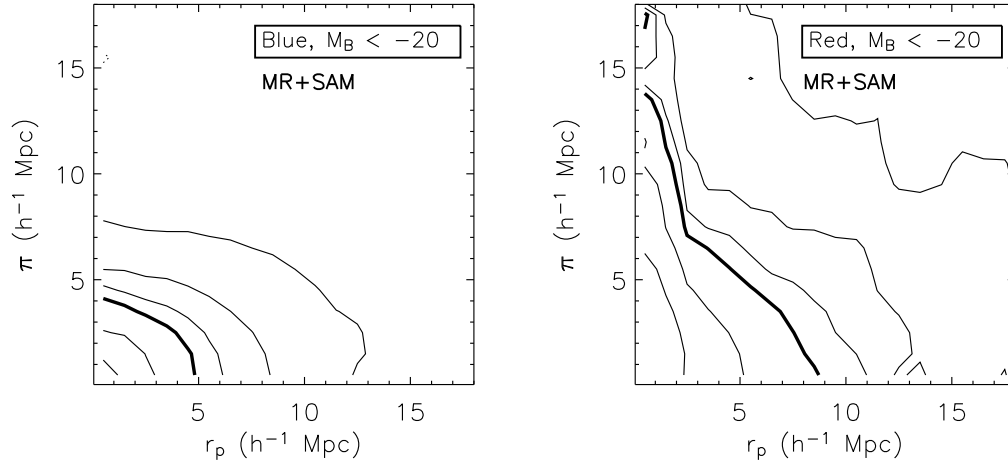


FIG. 15.— The two-dimensional correlation function,  $\xi(r_p, \pi)$ , for blue (left) and red (right) galaxies in the Millenium Run semi-analytic model mock galaxy catalogs (Croton et al. 2006) matched to the DEEP2 survey. A  $1 \times 1 h^{-1}$  Mpc boxcar smoothing has been applied in the figure, and contours levels are the same as in Figure 3. Almost no small scale redshift-space distortions are seen for blue galaxies, while red galaxies show strong fingers of god as well as coherent infall on large scales.

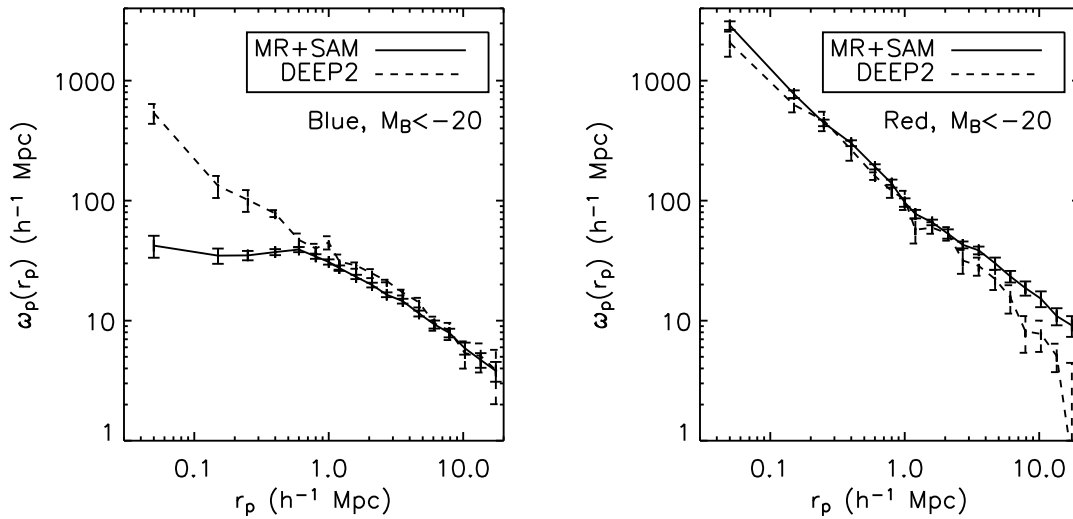


FIG. 16.— The projected correlation function,  $w_p(r_p)$ , for blue (left) and red (right) galaxies in the Millenium Run semi-analytic model mock catalogs (solid line) and the DEEP2 galaxy data (dashed line). There is a strong discrepancy between the model and the data for blue galaxies on small scales ( $r_p < 1 h^{-1}$  Mpc), where the model does not have enough blue galaxies. The red galaxy correlation function is too high on all scales in the model compared to the data.

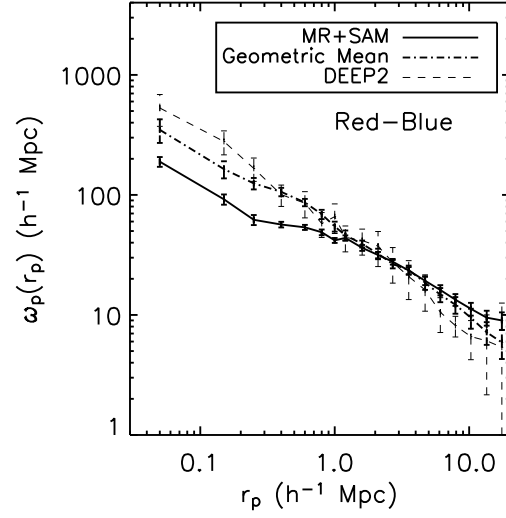


FIG. 17.— The projected cross-correlation function for blue and red galaxies in the Millenium Run semi-analytic model mock catalogs (solid line) and the DEEP2 galaxy data (thin dashed line). The geometric mean of the blue and red auto-correlation functions in the semi-analytic model is shown for comparison (dot-dash line). On small scales ( $r_p < 1 h^{-1}$  Mpc) the cross-correlation function in the model is significantly lower than both the geometric mean of the blue and red galaxies in the model and the cross-correlation function in the DEEP2 data.